TECTONICS, VOL. 23, TC5013, doi:10.1029/2003TC001559, 2004

Thermochronology of the modern Indus River bedload: New insight into the controls on the marine stratigraphic record

Peter D. Clift,[1,2] Ian H. Campbell,[3] Malcolm S. Pringle,[4,5] Andrew Carter,[6] Xifan Zhang,[7] Kip V. Hodges,[4] Ali Athar Khan,[8] and Charlotte M. Allen[3]

Received 3 July 2003; revised 14 June 2004; accepted 23 July 2004; published 16 October 2004.

[1] The Indus River is the only major drainage in the western Himalaya and delivers a long geological record of continental erosion to the Arabian Sea, which may be deciphered and used to reconstruct orogenic growth if the modern bedload can be related to the mountains. In this study we collected thermochronologic data from river sediment collected near the modern delta. U-Pb ages of zircons spanning 3 Gyr show that only ~5% of the eroding crust has been generated since India-Asia collision. The Greater Himalaya are the major source of zircons, with additional contributions from the Karakoram and Lesser Himalaya. The $^{39}Ar/^{40}Ar$ dating of muscovites gives ages that cluster between 10 and 25 Ma, differing from those recorded in the Bengal Fan. Biotite ages are generally younger, ranging 0–15 Ma. Modern average exhumation rates are estimated at ~0.6 km/m.y. or less, and have slowed progressively since the early Miocene (~20 Ma), although fission track (FT) dating of apatites may indicate a recent moderate acceleration in rates since the Pliocene (~1.0 km/m.y.) driven by climate change. The $^{39}Ar/^{40}Ar$ and FT techniques emphasize the dominance of high topography in controlling the erosional flux to the ocean. Localized regions of tectonically driven, very rapid exhumation (e.g., Nanga Parbat, S. Karakoram metamorphic domes) do not dominate the erosional record. *INDEX TERMS:* 8102 Tectonophysics: Continental contractional orogenic belts; 1625 Global Change: Geomorphology and weathering (1824, 1886); 1094 Geochemistry: Instruments and techniques; 1035 Geochemistry: Geochronology; 9320 Information Related to Geographic Region: Asia; *KEYWORDS:* Himalaya, Indus River, fission track, exhumation, erosion, thermochronology. **Citation:** Clift, P. D., I. H. Campbell, M. S. Pringle, A. Carter, X. Zhang, K. V. Hodges, A. A. Khan, and C. M. Allen (2004), Thermochronology of the modern Indus River bedload: New insight into the controls on the marine stratigraphic record, *Tectonics*, *23*, TC5013, doi:10.1029/2003TC001559.

1. Introduction

[2] Growth of topographic relief is at the center of feedback systems that link climate, tectonics and erosion. To fully understand the interdependency between these different processes we need to be able to reconstruct the topographic evolution of major mountain belts such as the Himalaya. However, this is difficult to achieve directly from present-day exposures as much of the record has been eroded away. Therefore we need to look into the sediment record to reconstruct the history of orogenic exhumation. In the case of the Himalaya this requires studying sediment from the Indus and Bengal Fan systems.

[3] Knowledge of contemporary Himalayan erosion is based on fluvial output [e.g., *Galy and France-Lanord*, 2001], or erosion indices integrating precipitation, stream power and shear stress [e.g., *Finlayson et al.*, 2002]. These studies reveal spatially variable and focused erosion that drives and maintains localized rock uplift [e.g., *Zeitler et al.*, 2001]. It is also apparent that areas with highest topographic relief tend to have higher erosion rates, so that these areas might be expected to dominate the sediment record. In this study we employ thermochronology to characterize the exhumation in the western Himalaya using contemporary Indus River sediment. We assess how well topographic signals associated with areas of high erosion can be recovered and linked to the original source area. In this respect the Indus River is well served because the exhumation history of the catchment ranges has been described in some detail by earlier thermochronological studies.

[4] The results from this study have implications for the interpretation of the marine stratigraphic record deposited in the Arabian Sea. The sediments of the Indus Fan are expected to contain a complete record of the exhumation history of the western Himalaya, with implications for the climatic and tectonic evolution of the area since the start of India-Asia collision. Decoding this record may allow models proposing links between the tectonic evolution of the

[1]Department of Geology and Geophysics, Woods Hole Oceanographic Institution, Woods Hole, Massachusetts, USA.
[2]Now at Department of Geology and Petroleum Geology, Kings College, University of Aberdeen, Aberdeen, UK.
[3]Institute of Advanced Studies, Research School of Earth Sciences, Australian National University, Canberra, ACT, Australia.
[4]Department of Earth, Atmospheric and Planetary Sciences, Massachusetts Institute of Technology, Cambridge, Massachusetts, USA.
[5]Also at Scottish Universities Environmental Research Centre (SUERC), East Kilbride, UK.
[6]School of Earth Sciences, University and Birkbeck College London, London, UK.
[7]Department of Geology and Geophysics, University of Wisconsin-Madison, Madison, Wisconsin, USA.
[8]Department of Geology, University of Karachi, Karachi, Pakistan.

0278-7407/04/2003TC001559

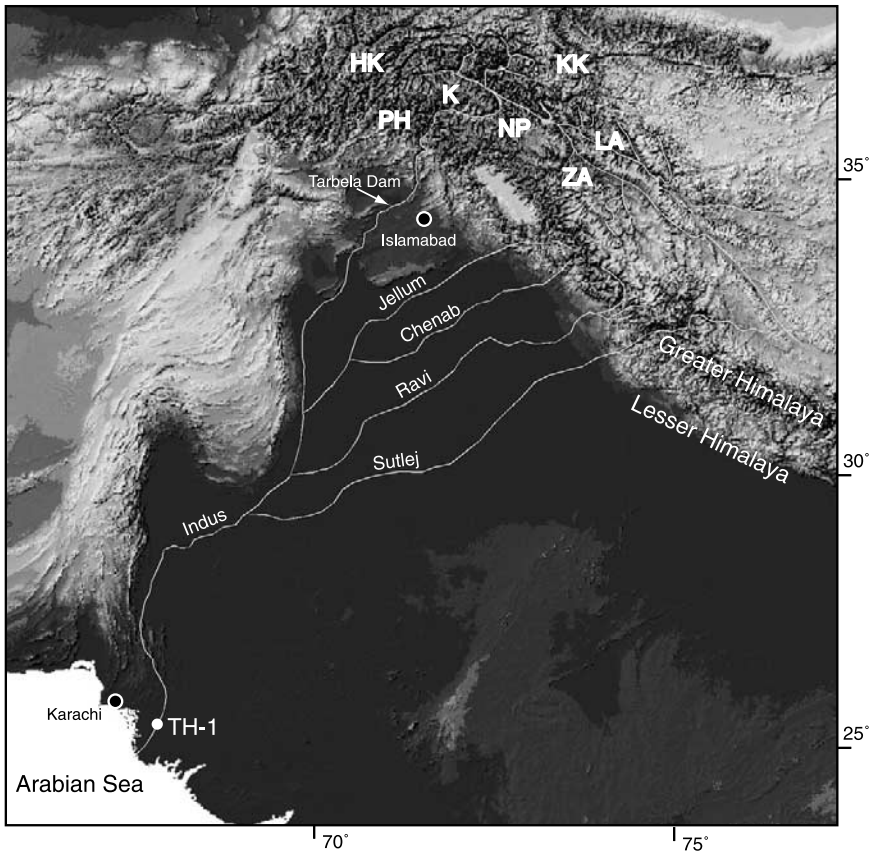

Figure 1. Digital topographic map of the Indus drainage basin showing sample location, the geometry of the Indus River and the name of major ranges and tributaries named in the text. Abbreviations are as follows: HK, Hindu Kush; PH, Pakistan Himalaya; K, Kohistan; NP, Nanga Parbat; KK, Karakoram; LA, Ladakh; ZA, Zanskar.

mountains and the climate to be tested [e.g., *Harrison et al.*, 1992; *Molnar et al.*, 1993]. However, we first need to understand the relationship between the modern bedload of the river and its source terrains.

[5] In this paper we present a series of thermochronometric measurements made from a single sample of sand taken from the main course of the Indus River at Thatta, close to the present delta mouth (Figure 1). This sample is presumed to be representative of the sediment now being delivered to the Arabian Sea by the Indus River, thus allowing the relationship between the bedload of the Indus River, the modern topography of the drainage, and its exhumation history to be examined. We have analyzed different mineral grains from this sand in order to understand the use of each mineral group as a provenance tool and to explore the history of crustal accretion, metamorphism and exhumation within the western Himalaya. Although thermochronometric data from outcrop studies are used to help interpret the detrital grain ages we recognize that outcrop studies necessarily cover only a limited region, which may or may not be representative of the entire region, especially as geologists tend to sample areas that have the most ready access. The bedload of the river however derives grains from all the actively eroding parts of the drainage, making this potentially a more representative sample of the catchment bedrock sources.

2. Analytical Methods

[6] In this study three different thermochronometric methods are employed to monitor the source of sediment to the lower Indus. Each method is sensitive to a different temperature range and therefore different stages of source thermal evolution: The high-temperature U-Pb data record zircon crystallization ages, while $^{39}Ar/^{40}Ar$ dating of mica grains records postmetamorphic cooling and exhumation through intermediate depths and temperatures. Finally, low-temperature apatite fission track ages are used to monitor exhumation and cooling in the uppermost part of the crust. The benefit of using three different thermochronometers is that it enables a more complete picture of the sediment source to be developed and reduces lithological bias associated with the use of a single mineral phase.

[7] Zircon U-Pb dating reflects the time of zircon growth, which in most cases is the rock crystallization age. The U-Pb system is mostly unaffected by high-grade metamorphism and is effectively stable up to ~750°C [*Cherniak and Watson*, 2001; *Carter and Bristow*, 2000]. Detrital zircon

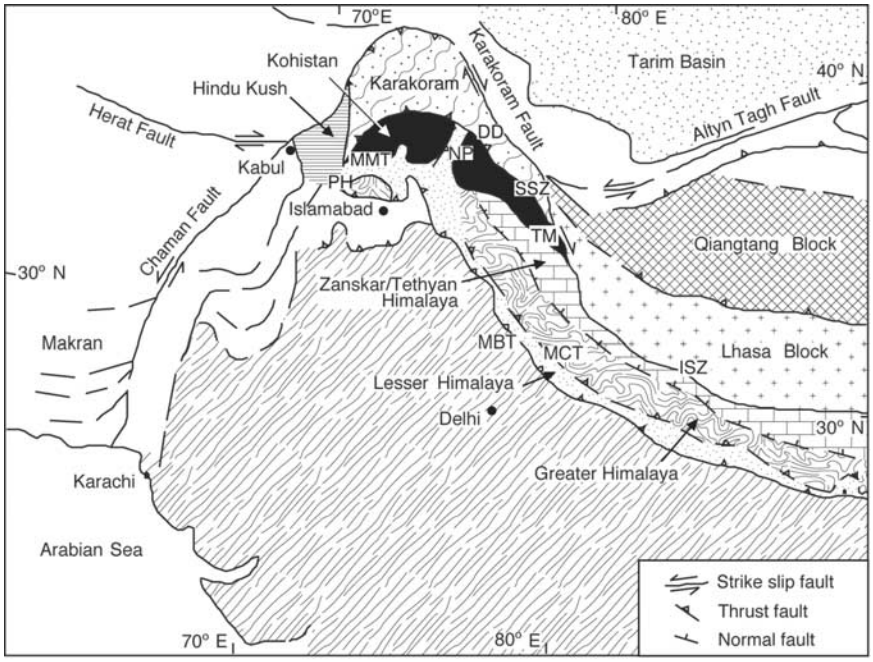

Figure 2. Regional geological map of the Indus drainage basin, showing the major units that provide sediment to the river. Abbreviations are as follows: NP, Nanga Parbat; DD, Dassu Dome; TM, Tso Morari; SSZ, Shyok Suture Zone; ISZ, Indus Suture Zone; MMT, Main Mantle Thrust; MCT, Main Central Thrust; MBT, Main Boundary Thrust.

U-Pb ages from river sediments are therefore expected to be representative of the range of crustal ages within the drainage basin. In contrast, the $^{39}Ar/^{40}Ar$ age of a detrital mica typically reflects the time at which that mineral cooled through 250–350°C for biotite, 350–400°C for muscovite [*Hodges*, 2003] following peak metamorphism. The technique has proven useful in dating metamorphic events throughout the Himalaya and Karakoram (Figure 2), two separate ranges that show significantly different cooling histories [e.g., *Searle*, 1996; *Guillot et al.*, 1999]. The $^{39}Ar/^{40}Ar$ method has also been successfully used as a provenance tool dating the foreland sediments [*Najman et al.*, 2002]. The low-temperature apatite fission track method, which records cooling through ~125–60°C over timescales of 1–10 m.y. [*Green et al.*, 1989] is particularly sensitive to exhumation driven by erosion and has been widely used in Himalayan exhumation studies. It is also an effective provenance tool [e.g., *Carter*, 1999] and has been used in previous studies of Indian Ocean sediments recovered by Ocean Drilling Program (ODP) [*Corrigan and Crowley*, 1990].

[8] U-Th-Pb isotopic compositions of zircons were analyzed at the Australian National University, Canberra, using Excimer Laser Ablation Inductively Coupled Plasma Mass Spectrometry (ELA-ICP-MS). The zircons were separated from the bulk sediment by conventional magnetic and heavy liquid separation techniques. The extracted zircons were mounted in epoxy resin and polished. Optical photomicrographs were used to map and select least-fractured and inclusion free zircons for analysis. Dating by ELA-ICP-MS followed a procedure described by *Ballard et al.* [2001]. Samples were ablated with a pulsed 193 μm ArF Lambda-Physik LPX 1201 UV Excimer laser with constant 100mJ energy and a repetition rate of 5 Hz. The laser makes a pit in the crystal 29 μm in diameter and ~20 μm deep, much deeper than the ~2 μm depth formed by ion probe methodologies. A mixed Ar-He (with minor H_2) carrier gas transported the ablated material from the sample cell into a flow homogenizer to an Agilent 7500 ICP-MS. Counts for ^{39}Si, ^{91}Zr, ^{31}P, ^{178}Hf, ^{206}Pb, ^{207}Pb, ^{208}Pb, ^{232}Th ^{235}U, ^{238}U and seven rare earth elements were collected in time-resolved, single point-per-peak mode. Measured ^{235}U is used in preference to ^{238}U for zircons with U > 2,500 ppm to avoid dead-time problems associated with the measurement of ^{238}U at high count rates, and in this rare circumstance $^{206}Pb/^{238}U$ is calculated from the measured $Pb^{206}Pb/^{235}U$, assuming $^{238}U/^{235}U = 137.88$. In the common case, $^{207}Pb/^{235}U$ is calculated from the measured $^{207}Pb/^{238}U$ for zircon with U < 2,500 ppm, because ^{238}U is measured with higher precision than ^{235}U. Because of a high ^{204}Hg blank, believed to reside in the carrier gas, ^{204}Pb was not measured.

[9] The integration time for the three Pb isotopes was 50 ms, 25 ms for U and Th, and for all other isotopes it was 5 ms with a total mass sweep time of 0.32 s. Background was measured for 20 s with the laser turned off, and the sample measured for a further 40 s with the laser turned on, giving ~130 mass scans for a penetration depth of ~25 μm. After triggering the laser, it took approximately 10 mass scans to reach a steady signal, so the initial data were excluded from data reduction. Depth-dependent interelement fractionation of Pb, Th and U [e.g.,

Table 1 (Representative Sample). Analytical Data From ICP-MS Laser Analysis of Zircon Grains for U-Pb Geochronology (The full Table 1 is available in the HTML version of this article at http://www.agu.org/pubs/current/tc/)

					$^{206}Pb/^{238}U$ Ratios						$^{207}Pb/^{235}U$ Ratios			$^{207}Pb/^{206}Pb$ Ratios		
Grain Number	Pb*, ppm	U, ppm	Atomic Th/U	P, ppm	Uncorrected $^{206}Pb/^{238}U$ Ratio	±SE	^{208}Pb Corrected $^{206}Pb^*/^{238}U$ Ratio	^{207}Pb Corrected $^{206}Pb^*/^{238}U$ Ratio	% Common ^{206}Pb Using ^{208}Pb	% Common ^{206}Pb Using ^{207}Pb	Uncorrected $^{207}Pb/^{235}U$ Ratio	±SE	^{208}Pb Corrected $^{207}Pb^*/^{235}U$ Ratio	Uncorrected $^{207}Pb/^{206}Pb$ Ratio	±SE	^{208}Pb Corrected $^{207}Pb^*/^{206}Pb^*$ Ratio
001	93.5	251.8	0.644	737	0.32924	0.00081	0.32959	0.32900	−0.10	0.07	5.11779	0.02026	5.18791	0.11274	0.00035	0.11410
002	35.3	437.2	0.368	956	0.07944	0.00024	0.07959	0.07952	−0.18	−0.10	0.61591	0.00567	0.64190	0.05623	0.00049	0.05845
003[a]	36.0	339.8	0.067	452	0.11278	0.00059	0.11150	0.10590	1.14	6.50	1.75146	0.02049	1.59005	0.11263	0.00118	0.10344
004	182.8	548.8	0.648	356	0.29797	0.00062	0.29855	0.29458	−0.19	1.15	4.61058	0.01406	4.71220	0.11222	0.00025	0.11441
005[a]	78.6	385.0	0.341	382	0.20107	0.00120	0.20036	0.18952	0.35	6.09	3.50867	0.02424	3.42526	0.12656	0.00044	0.12395
006	34.5	1495.5	1.098	116	0.01877	0.00015	0.01837	0.01835	2.17	2.26	0.17189	0.00298	0.12220	0.06642	0.00101	0.04829
007	40.4	1480.9	0.126	210	0.02884	0.00011	0.02882	0.02884	0.09	0.02	0.19849	0.00259	0.19701	0.04991	0.00062	0.04956
008[a]	274.1	751.4	0.087	457	0.36670	0.00195	0.36674	0.36601	−0.01	0.19	6.34028	0.03621	6.35525	0.12540	0.00026	0.12566
009	175.2	266.5	0.805	307	0.53389	0.00114	0.53475	0.53934	−0.16	−1.01	13.64707	0.04216	13.96436	0.18539	0.00041	0.18895
010	82.2	163.2	0.503	155	0.44820	0.00176	0.44605	0.44204	0.48	1.39	10.11027	0.09337	9.89645	0.16360	0.00137	0.16067
011	45.6	359.2	0.505	334	0.11984	0.00027	0.11991	0.12002	−0.05	−0.15	1.03181	0.00604	1.04794	0.06244	0.00034	0.06335
012	4.8	224.8	1.177	290	0.01730	0.00009	0.01723	0.01728	0.37	0.13	0.11759	0.00216	0.11298	0.04930	0.00087	0.04747
013	65.2	186.2	0.596	987	0.31541	0.00071	0.31590	0.31338	−0.16	0.65	4.92272	0.01763	5.01136	0.11320	0.00031	0.11500
014	30.3	222.1	0.511	200	0.12825	0.00046	0.12753	0.12783	0.56	0.32	1.19824	0.01229	1.13538	0.06776	0.00065	0.06446
015	55.9	293.8	1.261	455	0.15023	0.00050	0.15017	0.15012	0.04	0.07	1.44383	0.01046	1.51954	0.06971	0.00045	0.07307
016	5.7	1670.6	1.086	105	0.00279	0.00002	0.00275	0.00273	1.60	2.17	0.02448	0.00087	0.01971	0.06362	0.00223	0.05198
017	16.0	41.8	1.193	185	0.30518	0.00101	0.30783	0.30493	−0.86	0.08	4.45152	0.03532	4.86838	0.10579	0.00076	0.11455
018[a]	122.4	1433.7	1.297	614	0.06835	0.00068	0.06993	0.06752	−2.25	1.23	0.61564	0.00741	0.85035	0.06532	0.00045	0.08776
019	140.7	420.8	0.604	275	0.30084	0.00106	0.29988	0.29784	0.32	1.01	4.64089	0.02550	4.59927	0.11188	0.00047	0.11099
020	2.0	212.0	0.997	169	0.00782	0.00005	0.00781	0.00780	0.06	0.21	0.05251	0.00152	0.05323	0.04871	0.00138	0.04935
021	113.2	327.9	0.330	515	0.32810	0.00092	0.32682	0.32736	0.39	0.23	5.13914	0.02752	4.94925	0.11360	0.00052	0.10986
022	2.4	290.3	0.858	982	0.00720	0.00004	0.00708	0.00712	1.74	1.21	0.05625	0.00155	0.04287	0.05664	0.00152	0.04385
023	4.8	33.4	0.680	646	0.13007	0.00073	0.12999	0.12978	0.06	0.22	1.20598	0.01781	1.21024	0.06725	0.00092	0.06747
024	79.5	231.8	0.661	411	0.30534	0.00112	0.30625	0.30219	−0.30	1.04	4.77430	0.02560	4.90361	0.11340	0.00044	0.11612
025[a]	18.7	117.3	1.119	139	0.12938	0.00073	0.12827	0.12910	0.86	0.22	1.19675	0.01198	1.08976	0.06709	0.00055	0.06149
026	45.1	279.8	0.598	225	0.14778	0.00045	0.14713	0.14750	0.44	0.19	1.43018	0.01062	1.38666	0.07019	0.00047	0.06821
027	15.5	39.8	0.828	317	0.33138	0.00111	0.33092	0.33149	0.14	−0.03	5.14216	0.04247	5.12827	0.11254	0.00085	0.11227
028	122.4	394.7	0.198	383	0.30802	0.00099	0.30818	0.30538	−0.05	0.87	4.79064	0.02120	4.83234	0.11280	0.00034	0.11367
029	65.4	209.1	0.432	569	0.29456	0.00107	0.29443	0.29081	0.04	1.29	4.56490	0.02655	4.59988	0.11240	0.00051	0.11316
030[a]	38.1	1871.9	1.422	1692	0.01562	0.00007	0.01579	0.01560	−1.11	0.07	0.10465	0.00088	0.12940	0.04860	0.00036	0.05931
031	164.0	487.7	0.190	582	0.33204	0.00068	0.33186	0.33177	0.05	0.08	5.20266	0.01764	5.19295	0.11364	0.00031	0.11345
032	49.2	149.0	0.952	473	0.27480	0.00062	0.27402	0.27489	0.28	−0.03	3.66120	0.01551	3.61183	0.09663	0.00035	0.09545
033[a]	56.3	723.6	0.102	662	0.08143	0.00318	0.07965	0.07625	2.24	6.80	1.23031	0.04845	1.01287	0.10957	0.00059	0.09222
034	4.2	228.4	0.798	339	0.01623	0.00011	0.01610	0.01617	0.84	0.40	0.11491	0.00293	0.10555	0.05134	0.00126	0.04738
035	5.0	187.7	0.623	199	0.02467	0.00013	0.02453	0.02460	0.55	0.29	0.17526	0.00350	0.16293	0.05153	0.00099	0.04811
036[a]	56.3	419.7	0.731	1841	0.11823	0.00121	0.11534	0.11653	2.50	1.45	1.22447	0.02341	0.92272	0.07512	0.00121	0.05779
037	15.6	1192.4	1.934	28	0.00901	0.00003	0.00905	0.00901	−0.38	0.05	0.05910	0.00069	0.06750	0.04755	0.00054	0.05389
038	5.6	315.2	0.522	301	0.01678	0.00011	0.01673	0.01666	0.26	0.72	0.12485	0.00534	0.12076	0.05397	0.00228	0.05231
039	98.9	301.7	0.587	550	0.29705	0.00136	0.29746	0.29328	−0.14	1.29	4.62995	0.03219	4.66946	0.11304	0.00059	0.11390
040[a]	88.5	476.1	1.671	227	0.13516	0.00038	0.13491	0.13465	0.18	0.38	1.29383	0.01158	1.36070	0.06943	0.00059	0.07273
041	40.4	111.1	0.811	768	0.31132	0.00082	0.31028	0.30849	0.34	0.92	4.89868	0.02356	4.80511	0.11412	0.00046	0.11219
042	3.9	24.7	1.250	200	0.12595	0.00074	0.12551	0.12553	0.35	0.33	1.17064	0.02226	1.15354	0.06741	0.00122	0.06650

[a]Grain excluded from further consideration on the basis of criteria laid out in section 2.1.
[b]For speed of calculation, $^{207}Pb/^{206}Pb$ ages of zircons <150 Ma were not calculated.

Hirata and Nesbitt, 1995; *Horn et al.*, 2000], was corrected by reference to multiple measurements of standard zircon TEMORA and NIST612 silicate glass [*Pearce et al.*, 1997; *Black et al.*, 2000]. Measured $^{207}Pb/^{206}Pb$, $^{206}Pb/^{238}U$ and $^{208}Pb/^{232}Th$ ratios in TEMORA and $^{232}Th/^{238}U$ in NIST612 were averaged over the analytical period and used to calculate correction factors for each mass sweep down the ablated hole. These factors were applied to each mass scan to correct for instrumental mass bias and depth-dependent elemental and isotopic fractionation. Common Pb was determined by the ^{208}Pb method (the difference between the measured and expected $^{208}Pb/^{206}Pb$, given a preliminary $^{206}Pb/^{238}U$ age and Th/U [*Compston et al.*, 1984]) and the calculated amount subtracted, assuming a common Pb composition from the age-dependent Pb model of *Cumming and Richards* [1975]. Common ^{206}Pb is generally less than 1% of total ^{206}Pb. Given the age of the rocks analyzed here, model common Pb compositions do not vary greatly, and, at this level of common Pb, the model selected is irrelevant in terms of the calculated age (affecting a maximum change of 0.2%). In most cases, the resulting ratios were nearly concordant (see criteria below).

[10] Ages are calculated from data collected from regions free of inclusions and with a flat isotope response. Only analyses that were at least 10 mass scans wide were interpreted. In cases where a distinct core and rim were intersected (i.e., representing an original magmatic event and a later metamorphic overprint), one laser ablation might produce two results. Once the data were compiled, an analysis was rejected for interpretation on the basis of the following: (1) the observed variance in $^{206}Pb/^{238}U$ or $^{207}Pb/^{206}Pb$ (depending if the grain is > or <1200 Ma) is more than three times that calculated from counting statistics (this procedure omits grains that record mixed ages), or (2) the grain is deemed to be discordant. Grains >400 Ma are deemed concordant if their ^{208}Pb-based common Pb-$^{206}Pb/^{238}U$ corrected age, divided by their ^{208}Pb-based common Pb-$^{207}Pb/^{206}Pb$ age, is 1 ± 0.1 including uncertainties. For grains <400 Ma, the same procedure is employed except that $^{207}Pb/^{235}U$ is used instead of $^{207}Pb/^{206}Pb$. Both procedures are theoretically equivalent, but this change in concordance criteria is desirable because a given percentage error in the $^{207}Pb/^{206}Pb$ measurement results in a much larger error in the calculated age than the equivalent error in the age calculated from $^{206}Pb/^{238}U$. As a consequence, the percentage of discordant grains appears to increase in detrital zircon suites as the grains become younger if the $^{206}Pb/^{238}U$-$^{207}Pb/^{206}Pb$ method is used to test for concordance. This effect is unlikely to be real because young grains have less time to become metamict and are therefore less likely to lose Pb. There are two solutions to this problem, either systematically relaxing the concordance criteria as grains become younger or using $^{206}Pb/^{238}U$-$^{207}Pb/^{235}U$ as the concordance test for the most affected grains (those under 400 Ma). The latter is prefer because similar percentage errors in the measured $^{206}Pb/^{238}U$ and $^{207}Pb/^{235}U$ lead to errors in the calculated age that are more similar than the equivalent comparison for $^{206}Pb/^{238}U$-$^{207}Pb/^{206}Pb$ calculated ages, removing the need to relax the concordance criteria with decreasing age. In young grains the U/Pb ratios are much more precise than the $^{207}Pb/^{206}Pb$ ratios. In 612 homogenous glass analyses, the standard deviation in $^{206}Pb/^{238}U$ is 1%, and in $^{207}Pb/^{206}Pb$, 0.4%. Results of the U-Pb dating are shown in Table 1.

[11] $^{40}Ar/^{39}Ar$ laser fusion analyses were performed at the Massachusetts Institute of Technology (MIT) using procedures similar to those described by *Hodges and Bowring* [1995]. Prior to analysis, samples were irradiated in the C5 position of the McMaster University Nuclear Reactor for 10 hours with a total power of 20 MW. After fusion with an Ar-ion laser, the released gases were purified for 10 min with Al-Zr and Fe-Zr-V getters and then admitted to an MAP 215-50 mass spectrometer for Ar isotopic analysis using an electronic multiplier. The final data reduction was conducted with the program ArArCalc [*Koppers*, 2002]. The conversion efficiency of ^{39}K to ^{39}Ar was monitored using sanidine from the Taylor Creek rhyolite (TCR-2) with an assumed age of 28.34 Ma [*Renne et al.*, 1998]. Corrections for neutron-induced interference were made by the factors previously determined at MIT using K_2SO_4 and CaF_2 salts. Results are summarized in Tables 2a and 2b, and the complete set of analytical data is available in the auxiliary material[1].

[12] During the initial phase of this study, aliquots of ten crystals each of biotite or muscovite were fused per analysis. Later in the course of this study, significant software and hardware improvements in the noble gas laboratory at MIT made it possible to analyze individually the 200–400 μm diameter mica grains found in the sediment sample studied here. Therefore we analyzed a set of about fifty crystals each of muscovite and biotite using single crystal fusion techniques. In general, the integrated age of the 47 muscovite crystals fused individually compares well with the integrated age of the ~470 muscovites fused as 10 crystals at a time (22.4 ± 1.1 versus 25.1 ± 1.2 Ma, respectively; Tables 2a and 2b). However, the integrated age of the 46 biotite crystals fused individually is significantly younger than the integrated age of the ~490 biotite crystals fused 10 crystals at a time (20.8 ±1.6 versus 31.4 ± 2.7 Ma, respectively; Tables 2a and 2b). We suspect that this is mainly an artifact of the hand-picking process; fresh muscovite were abundant enough in this sample so that there was no significant difference between a population of ~50 or 500 grains, but in trying to pick a larger number of biotite crystals, we may have included a number of older, more altered grains that were selectively avoided when choosing the freshest looking grains for single crystal analysis.

[13] Apatite fission track analysis was performed at University College, London, UK. Polished grain mounts of apatite were etched with 5N HNO_3 at 20°C for 20 s to reveal the spontaneous fission tracks. Subsequently the uranium content of each crystal was determined by irradiation, which induced fission in a proportion of the ^{235}U. The induced tracks were registered in mica external detectors.

[1] Auxiliary material is available at ftp://ftp.agu.org/apend/tc/2003TC001559.

Table 2a. Summary of $^{40}Ar/^{39}Ar$ Laser-Fusion Analysis of Biotite From the Indus River[a]

Age, Ma	±2s, Ma	$^{40}Ar_{(rad)}$, %	$^{39}Ar_{(K)}$, mol
Bulk Laser Fusion (~10 Crystals Each)[b]			
16.17	±1.04	23.0	2.38E-14[c]
16.55	±2.61	14.8	1.66E-14
22.65	±1.09	30.1	1.77E-14
23.41	±2.18	24.7	2.01E-14
23.90	±2.21	26.4	2.12E-14
23.91	±1.59	19.5	1.30E-14
24.09	±1.14	32.7	2.21E-14
24.68	±2.68	22.0	1.46E-14
24.88	±3.54	25.9	1.32E-14
24.98	±0.66	32.2	3.12E-14
25.66	±3.29	15.8	9.57E-15
25.72	±2.93	19.5	1.27E-14
25.91	±0.95	43.8	3.13E-14
26.38	±2.76	16.4	1.30E-14
26.38	±4.05	18.6	1.32E-14
26.65	±0.84	34.9	2.02E-14
27.17	±0.98	29.2	2.02E-14
27.42	±2.81	18.4	9.85E-15
27.51	±2.21	30.9	1.33E-14
28.59	±3.76	22.9	9.77E-15
28.83	±2.53	26.9	1.55E-14
29.05	±3.08	20.7	1.62E-14
30.91	±3.25	21.6	1.56E-14
31.39	±2.55	24.6	1.40E-14
31.59	±5.17	19.4	9.71E-15
31.61	±3.24	30.1	1.49E-14
32.21	±3.70	16.6	1.15E-14
32.21	±2.11	35.0	1.53E-14
33.66	±3.08	26.8	9.21E-15
34.06	±4.76	16.7	9.15E-15
35.20	±2.42	26.0	1.07E-14
35.40	±4.12	24.3	8.86E-15
36.27	±1.62	29.9	1.93E-14
36.97	±3.14	24.9	1.42E-14
38.05	±2.77	30.8	1.33E-14
38.52	±3.33	31.5	1.36E-14
38.87	±4.59	24.7	8.40E-15
39.21	±5.14	14.7	7.61E-15
41.20	±7.14	19.5	6.68E-15
41.74	±2.60	25.9	1.34E-14
41.81	±4.03	23.4	7.27E-15
42.06	±2.63	22.8	6.88E-15
43.29	±3.50	27.9	6.82E-01
47.80	±5.62	23.7	5.62E-15
48.01	±7.34	21.6	5.93E-15
51.31	±6.77	19.5	5.17E-15
72.76	±5.09	54.2	1.16E-14
72.93	±11.32	18.4	5.56E-15
84.31	±3.22	42.5	8.60E-15
Single Crystal Laser Fusion (Black xls)			
2.90	±4.13	26.8	1.22E-15
3.95	±3.64	21.3	1.59E-15
4.23	±1.23	62.4	2.94E-15
4.43	±3.16	20.2	1.46E-15
5.22	±2.34	40.4	1.81E-15
5.79	±3.11	53.6	1.73E-15
5.81	±1.50	68.7	3.73E-15
6.85	±2.36	38.3	2.01E-15
11.42	±2.20	88.8	1.93E-15
11.77	±2.30	71.0	2.09E-15
11.97	±2.30	93.0	2.08E-15
12.08	±1.65	68.4	2.52E-15
16.44	±2.13	77.0	2.72E-15
17.61	±6.43	38.1	9.62E-16
21.12	±1.90	64.8	2.51E-15
27.78	±3.16	72.1	1.75E-15
32.56	±1.20	84.3	5.08E-15
33.53	±1.41	91.5	3.81E-15
35.16	±3.67	76.7	9.82E-16
37.20	±0.72	78.8	5.23E-15
43.52	±4.19	66.9	1.31E-15
51.50	±0.45	100.0	1.46E-15
109.14	±2.79	95.2	1.65E-15
112.44	±2.00	89.7	2.58E-15
Single Crystal Laser Fusion (Brown xls)[d]			
1.94	±1.06	14.7	5.62E-15
2.29	±1.35	62.5	3.48E-15
2.30	±1.80	31.7	2.26E-15
2.39	±0.85	51.8	4.71E-15
2.54	±1.19	44.9	3.56E-15
2.99	±3.37	31.0	1.52E-15
3.25	±1.36	59.4	4.34E-15
4.40	±1.50	40.9	4.27E-15
4.92	±1.26	72.2	3.40E-15
5.46	±1.26	73.6	4.17E-15
5.55	±1.40	26.2	3.33E-15
5.86	±2.05	91.4	2.44E-01
8.26	±1.12	56.7	4.66E-15
10.50	±0.98	75.0	4.06E-15
10.54	±1.18	61.9	4.19E-15
11.04	±1.68	61.4	2.53E-15
13.17	±0.82	84.2	8.10E-15
13.21	±3.12	44.1	1.58E-01
15.31	±3.54	38.6	2.35E-15
20.61	±1.70	58.7	2.77E-15
56.87	±1.07	92.0	6.30E-15
86.10	±0.82	97.8	6.74E-15

[a]Ages relative to TCR-2 Sanidine at 28.34 Ma. Here $^{40}Ar_{(rad)}$ and $^{39}Ar_{(K)}$ denote radiogenic and K-derived argon, respectively. Complete analytical data are reported in auxiliary material. Error in flux monitor, *J*, of approximately 1% per sample packet is not incorporated into individual ages reported here, to facilitate proper calculation of each intrasample age distribution.

[b]Age average is 31.367 ± 2.71. TGA (Ma) equals ~490 crystals.

[c]Read 2.38E-14 as 2.38×10^{14}.

[d]Age average is 20.77 ± 1.6. TGA (Ma) equals 46 crystals.

The sample for this study was irradiated in the thermal facility of the Hifar Reactor at Lucas Heights, Australia. The neutron flux was monitored by including Corning glass dosimeter CN-5, with a known uranium content of 11 ppm, at either end of the sample stack. After irradiation, sample and dosimeter mica detectors were etched in 40% HF at 20°C for 45 min. Only crystals with sections parallel to the c-crystallographic axis were counted, as these crystals have the lowest bulk etch rate. To avoid biased results through preferred selection of apatite crystals the sample was systematically scanned and each crystal encountered with the correct orientation was analyzed, irrespective of track density. The results of the fission track analysis are presented in Table 3.

3. U-Pb Dating of Zircons

[14] The results of zircon dating sample TH-1 are shown in Figure 3, which plots the entire range of U-Pb crystal-

Table 2b. Summary of $^{40}Ar/^{39}Ar$ Laser-Fusion Analysis of Muscovite From the Indus River[a]

Age, Ma	±2s, Ma	$^{40}Ar_{(rad)}$, %	$^{39}Ar_{(K)}$, mol
Bulk Laser Fusion (~10 Crystals Each)[b]			
7.96	±1.14	37.3	9.93E-15[c]
12.23	±1.26	65.6	3.14E-14
12.29	±1.61	61.2	3.23E-14
12.31	±1.67	60.7	2.06E-14
12.54	±0.50	58.9	1.66E-14
13.88	±1.87	72.3	3.17E-14
13.89	±1.42	46.0	1.45E-14
14.72	±1.29	76.5	4.44E-14
14.95	±1.63	73.4	2.77E-14
16.06	±1.47	64.8	2.51E-14
16.26	±1.44	82.9	6.07E-14
17.66	±0.54	88.0	9.13E-14
17.69	±1.26	64.9	2.62E-14
17.72	±1.09	58.1	1.56E-14
18.26	±1.02	72.2	4.24E-14
18.91	±1.41	83.0	7.85E-14
19.34	±1.14	82.9	4.90E-14
19.55	±1.21	84.9	5.41E-14
19.99	±0.46	87.6	8.59E-14
20.71	±0.66	87.6	4.86E-14
20.89	±0.91	87.4	6.04E-14
21.16	±0.71	87.0	4.82E-14
22.79	±0.46	90.6	8.03E-14
23.02	±0.93	89.4	5.69E-14
23.73	±2.99	85.7	3.28E-01
24.68	±1.44	87.7	4.75E-14
25.00	±1.19	87.0	5.48E-14
25.56	±2.07	85.4	5.81E-14
25.76	±1.67	85.9	2.89E-14
26.19	±1.57	83.9	3.77E-14
26.90	±1.39	89.1	5.17E-14
28.78	±1.92	84.3	3.34E-14
29.08	±0.73	89.1	5.42E-14
29.13	±1.19	84.7	4.47E-14
29.42	±0.84	88.9	5.12E-14
30.77	±0.86	88.8	4.42E-14
30.91	±0.69	90.2	5.40E-14
32.07	±1.85	89.0	4.16E-14
34.81	±0.53	96.1	4.76E-14
35.49	±1.59	83.7	3.07E-14
35.64	±1.70	82.7	2.49E-14
36.17	±1.76	93.2	3.19E-14
39.33	±1.02	92.7	5.10E-14
41.82	±1.23	94.1	3.25E-14
50.99	±1.50	90.5	3.68E-14
52.29	±1.08	89.4	3.54E-14
102.33	±3.43	93.2	1.21E-14
Single Crystal Laser Fusion[d]			
1.29	±2.7	12.9	1.88E-15
4.08	±0.78	60.4	5.87E-15
4.18	±1.22	66.8	3.09E-15
5.06	±0.08	99.6	4.97E-15
7.98	±1.08	69.4	3.55E-15
9.09	±2.79	26.0	1.74E-15
9.59	±0.70	77.9	6.97E-15
10.39	±3.40	49.7	1.47E-15
11.44	±2.91	45.1	1.30E-15
12.41	±1.08	62.6	5.26E-15
12.55	±3.41	39.0	2.11E-15
12.65	±1.45	67.9	4.29E-15
14.87	±0.86	86.1	5.70E-15
15.15	±2.67	71.5	1.80E-15
15.19	±0.87	80.6	5.26E-15
15.19	±1.35	74.3	3.68E-15
15.41	±0.53	83.3	9.66E-15
15.42	±1.46	75.4	3.48E-15
15.66	±3.28	61.4	1.26E-15
15.71	±0.97	75.1	5.06E-15
15.99	±0.60	87.0	1.32E-14
16.20	±2.00	85.1	3.52E-15
16.27	±0.86	77.7	6.71E-15
16.37	±1.48	83.8	3.66E-15
17.05	±2.11	78.7	2.95E-15
17.39	±0.95	84.4	4.37E-15
18.13	±1.02	61.7	4.64E-15
18.36	±1.68	71.9	2.43E-15
19.44	±0.16	99.9	2.79E-15
19.89	±0.84	86.5	8.45E-15
20.86	±1.46	90.0	4.47E-15
20.99	±1.12	71.3	4.80E-15
21.42	±0.59	85.1	8.06E-15
21.66	±2.58	89.4	1.70E-15
22.80	±1.38	82.3	4.49E-15
22.97	±1.53	81.7	2.93E-15
23.17	±0.31	93.2	1.68E-14
23.17	±1.54	89.9	3.23E-15
23.94	±1.14	94.9	3.67E-15
24.71	±2.08	86.8	2.66E-15
26.55	±1.05	90.2	4.04E-15
28.02	±0.57	89.0	8.24E-15
30.53	±0.78	78.9	4.42E-15
33.43	±1.11	77.1	9.20E-15
38.27	±0.94	90.3	6.18E-15
124.31	±2.58	93.2	2.06E-15
203.05	±2.36	95.7	3.38E-15

[a]Ages relative to TCR-2 Sanidine at 28.34 Ma. Here $^{40}Ar_{(rad)}$ and $^{39}Ar_{(K)}$ denote radiogenic and K-derived argon, respectively. Complete analytical data are reported in auxiliary material. Error in flux monitor, *J*, of approximately 1% per sample packet is not incorporated into individual ages reported here, to facilitate proper calculation of each intrasample age distribution.

[b]Age average is 25.097 ± 1.19. TGA (Ma), equals ~470 crystals.

[c]Read 9.93E-15 as 9.93×10^{15}.

[d]Age average is 22.426 ± 1.08. TGA (Ma) equals 47 crystals.

lization ages, while Figure 4 shows in more detail the last 500 m.y. In each case the age histogram is shown together with ages derived by earlier U-Pb zircon studies from possible basement source regions. Indian plate sources are represented by the Greater and Lesser Himalaya [*Noble and Searle*, 1995; *Parrish and Hodges*, 1996; *Hodges et al.*, 1996; *DeCelles et al.*, 2000], Pakistan Himalaya (west of Nanga Parbat [*Zeitler and Chamberlain*, 1991; *Anczkiewicz et al.*, 2001], and the Nanga Parbat-Haramosh Massif [*Zeitler and Chamberlain*, 1991; *Zeitler et al.*, 1993]). U-Pb zircon ages from the Karakoram are derived from *Le Fort et al.* [1983], *Parrish and Tirrul* [1989], *Schärer et al.* [1990], *Searle et al.* [1990], and *Fraser et al.* [2001], while those from the Kohistan Arc and the Ladakh (Transhimalayan) Batholith are taken from *Honegger et al.* [1982], *Weinberg and Dunlap* [2000], *Schärer et al.* [1984], and *Zeilinger et al.* [2001]. *Dunlap and Wysoczanski* [2002] provide ages of volcanic rocks within the Shyok Suture on the southern edge of the Karakoram in Ladakh.

[15] Comparison with known U-Pb zircon ages of basement rocks allows the influence of specific regions to the Indus bedload to be assessed, although we note that there is

Table 3. Fission Track Analytical Data for Indus River Sediment, Sample TH-1[a]

	Value
Number of grains	19
Dosimeter, ρd	1.298
Dosimeter, Nd	7196
Spontaneous, ρd	0.075
Spontaneous, Nd	28
Induced, ρd	4.262
Induced, Nd	1601
Age dispersion, $P\chi^2$	<1
Age dispersion, RE%	85.8
Central age, Ma	3.7 ± 1.1
Age mode (n = 16), Ma	2.2 ± 0.6
Age mode (n = 3), Ma	14 ± 4

[a]Track densities ($\rho_{d,s,i}$) are ($\times 10^6$ tr cm^{-2}) with numbers of tracks counted ($N_{d,s,i}$), using Zeiss Axioplan microscope, 1250× total magnification, 100× dry objective. Analyses by external detector method using 0.5 for the $4\pi/2\pi$ geometry correction factor; only crystals with prismatic sections parallel to c-crystallographic axis analyzed. Irradiation in thermal facility of Risø Reactor, National Research Centre, Roskilde, Denmark (cadmium ratio for Au > 400) using dosimeter glass CN-5 to monitor neutron fluence. Ages calculated using ζCN5 = 339 ± 5 calibrated by >33 analyses of IUGS apatite age standards. $P\chi^2$ is probability for obtaining χ^2 value for v degrees of freedom, where v = no. crystals − 1. Central age is a modal age, weighted for different precisions of individual crystals.

potential for bias whereby the age characteristics of the Greater and Lesser Himalaya are much better known than other parts of the drainage, including the Karakoram, where coverage is less complete. The Hindu Kush in particular has no U-Pb zircon age control. However, earlier geochemical based provenance work on Indus River sediment suggests that the Hindu Kush is not a major supplier of sediment to the main river [*Clift et al.*, 2002a; *Lee et al.*, 2003], so that our inability to account for its influence should not lead to major errors in understanding the erosion patterns in the Indus drainage.

[16] The data presented in Figure 3 shows that the vast majority of zircon grains in the Indus River have crystallization ages much older than India-Asia collision at ~50 Ma, indicating that while that collision clearly deformed and metamorphosed large crustal blocks in the western Himalaya and Karakoram it was not responsible for the generation of large volumes of new crust. The age histogram in Figure 3a, contains several distinct age modes that extend as far back as the Achaean. The durability of the zircon U-Pb system means these older ages are mostly inherited or recycled grains and this is borne out by studies on the Greater Himalayan rocks that have shown the protoliths had an east African origin [*DeCelles et al.*, 2000]. Although these ages have no direct significance in terms of Himalayan growth, they are useful for provenance reconstruction. The zircon U-Pb ages measured on Greater and Lesser Himalayan rocks contain the same range of Proterozoic and Achaean ages as the Indus sediment sample (Figures 3b–3g). This correspondence suggests a significant sediment flux from Greater and Lesser Himalayan sources to the Indus River. Nonetheless, it is also possible that some material may be derived from the Dassu Dome and other metamorphic complexes in the southern Karakoram, which has also yielded Proterozoic zircon U-Pb ages [*Fraser et al.*, 2001]. This region is affected by strong erosion and has high exhumation rates [5–7 km/m.y.; *Poupeau et al.*, 1991; *Villa et al.*, 1996]. The role of the Southern Karakoram Metamorphic Belt (SKMB) as a sediment source to the Indus River has also been inferred in earlier provenance studies [*Clift et al.*, 2002a; *Lee et al.*, 2003].

[17] Grains dated at <200 Ma match several basement ages measured in the Karakoram, although the Kohistan Arc may also be a source of grains of that age. These areas are the only clear source of recent crustal accretion in the western Himalaya. Detrital peaks at ~500 Ma and ~900 Ma match well with the age spectrum for the Greater Himalaya and are interpreted to reflect erosion from these sources. The ~500 Ma peak in particular forms a good match with the inherited zircons found in the granites of the Zanskar Himalaya [*Noble and Searle*, 1995], representing some of the highest topography in the Indus drainage.

[18] More detailed provenance conclusions may be reached by focusing on only the last 500 m.y. (Figure 4). In Figure 4 the importance of grains dated at <140 Ma can be seen. Although, there are grains dated at 400–500 Ma,

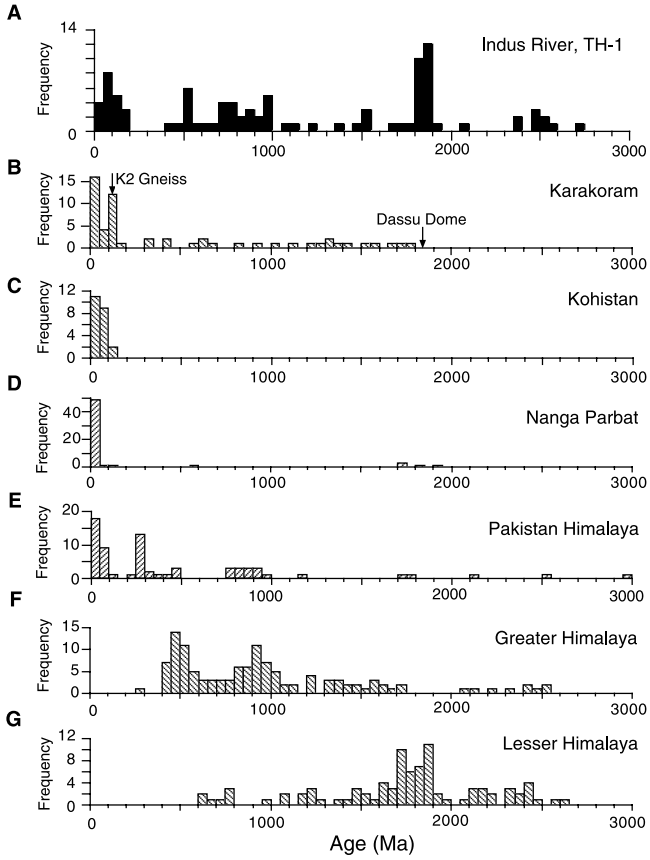

Figure 3. (a) Histogram of zircon U-Pb ages since 3.0 Ga derived from the Indus River at Thatta. U-Pb zircon age spectra for a series of potential source terrains is shown for (b) Karakoram, (c) Kohistan, (d) Nanga Parbat, (e) Pakistan Himalaya, (f) Greater Himalaya, and (g) Lesser Himalaya. Origin of source age data is provided in text.

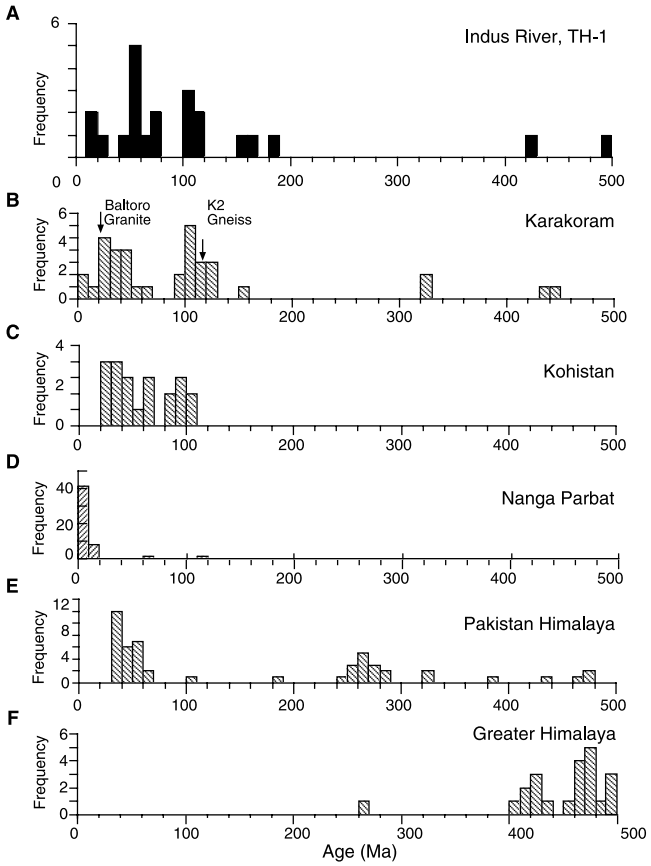

Figure 4. (a) Histogram of zircon U-Pb ages since 500 Ma derived from the Indus River at Thatta, showing the generally good fit between young U-Pb ages and known magmatic events constrained by U-Pb zircon dating in the Karakoram, but the general scarcity of grains with the 400–500 Ma age of the Greater Himalaya [*DeCelles et al.*, 2000]. Source U-Pb zircon spectra are from the (b) Karakoram, (c) Kohistan, (d) Nanga Parbat, (e) Pakistan Himalaya, and (f) Greater Himalaya.

coinciding with U-Pb zircon ages from Zanskar Greater Himalayan granites, these are less abundant than the younger grains, suggesting a greater erosional contribution from the Karakoram to the bedload. A number of age maxima can be identified, which correlate quite closely with possible source regions in the Karakoram. A peak at ~100–120 Ma correlates well with the known age of the K2 Gneisses [*Searle et al.*, 1990]. Similarly, grains yielding ages of 20–35 Ma match well with pegmatite and granite ages from the main Karakoram (Baltoro) Batholith [*Searle et al.*, 1989; *Schärer et al.*, 1990; *Fraser et al.*, 2001]. While these data do not prove that these areas are providing significant volumes of sediment, they are consistent with that hypothesis, which is further supported by earlier isotopic work on sediments from the Indus tributaries [*Clift et al.*, 2002a].

[19] Resolving the erosional component of the Kohistan Batholith using U-Pb zircon ages is difficult because of the significant overlap between the age of this unit and the Karakoram. While Kohistan must be contributing some material to the Indus bedload this unit experienced lower recent exhumation rates than seen in the SKMB [*Krol et al.*, 1996a; *Zeilinger et al.*, 2001], suggesting a lesser erosional contribution. This prediction is supported by geochemical provenance constraints [*Clift et al.*, 2002a; *Lee et al.*, 2003]. Contributions from the Transhimalaya further east (e.g., Ladakh Batholith) are similarly believed to be small, especially as fission track constraints from that region show even slower recent exhumation [*Sorkhabi et al.*, 1994; *Clift et al.*, 2002b]. Although the Pakistan Himalaya comprises some rocks with young zircon ages (30–70 Ma), which approximately match some of the detrital grains, the lack of any detrital ages in the 240–290 Ma range argues against this range being a major sediment supplier to the Indus (Figure 4d).

4. Ar-Ar Dating of Mica

[20] Differences between the single grain and 10-crystal batch analysis of micas are shown in Figure 5. As might be expected the muscovites show a similar average age for each method but with differences in the ability of the single grain method to detect small grain populations which are homogenized in the bulk approach. This is especially true of

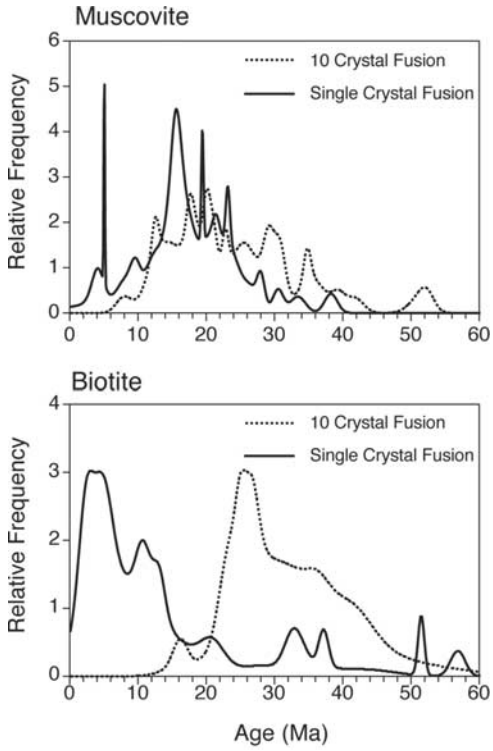

Figure 5. Comparison of $^{39}Ar/^{40}Ar$ age spectrum of both muscovite and biotite mica grains measured as single grains versus batch analysis of 10 grains at a time. Note that the batch analysis provides a reasonable average of the muscovite population it fails to identify the smaller grain populations with the youngest or oldest ages. The results of the single grain analysis for biotites shows a major shift to younger values compared to the bulk grain analysis.

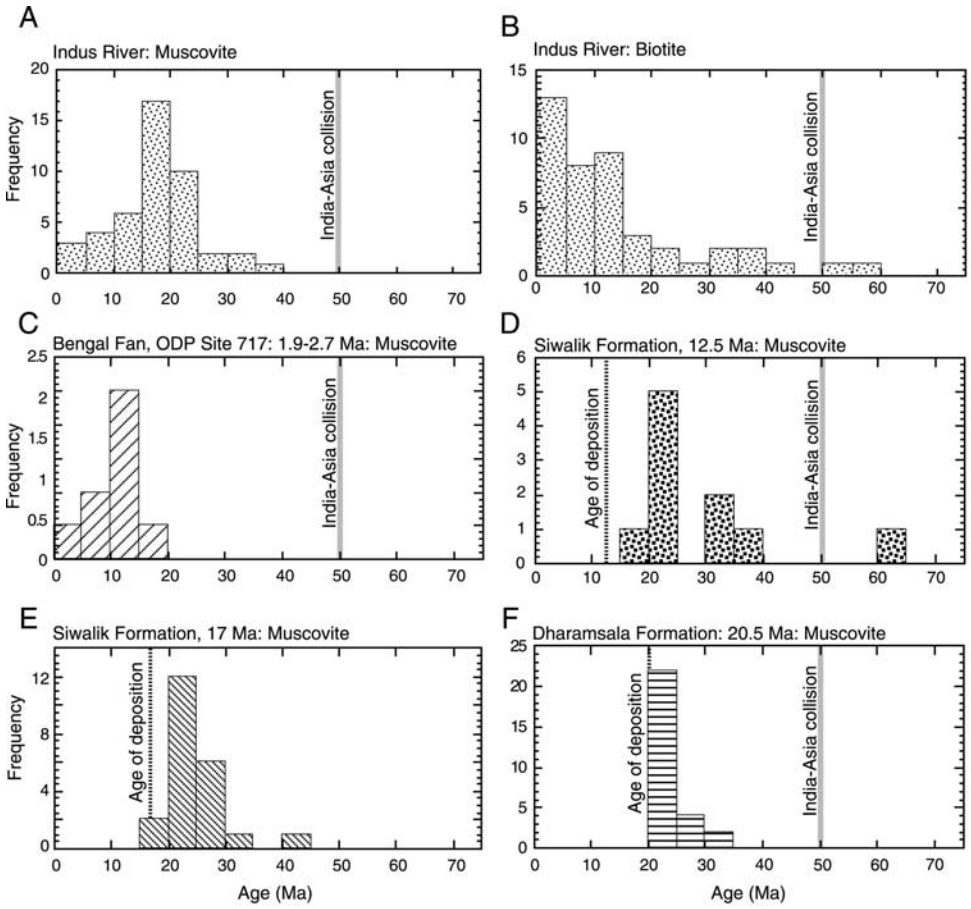

Figure 6. Range of $^{39}Ar/^{40}Ar$ ages measured from Indus River (a) biotite and (b) muscovites, compared to those known from (c) the Bengal Fan [*Copeland and Harrison*, 1990; *Copeland et al.*, 1990], and from the (d) 12.5 Ma Siwalik Group [*White et al.*, 2002], (e) 17 Ma Siwalik Group [*White et al.*, 2002], and the (f) early Miocene Dharamsala Formation [*Najman et al.*, 1997]. Both Siwalik and Kasauli Formations are foreland basin units, now imbricated within the Lesser Himalaya.

a sharp peak in ages around 5–6 Ma seen in the single grains that is not seen in the bulk analysis. The situation of the biotite grains is more problematic as there is a significant offset in the averages derived from each approach, with the single grain method highlighting a preference for grains <15 Ma, compared to the average of ~25 Ma seen in the batch analysis. The reason for this offset is not clear and seems to suggest sampling of different populations of grains. Figure 5 does highlight the potential dangers of assuming that batch analyses provide a good image of the age spectrum, as the importance of young grains and thus young source exhumation is not resolved in the batch method. Consequently we only use the single grain dates for further consideration in this study.

[21] The $^{39}Ar/^{40}Ar$ age distribution of detrital biotite and muscovite grains from TH-1 is shown in Figure 6. It is noteworthy that these two minerals have quite different age distributions, with the principal of the age distributions at 0–15 Ma and 15–25 Ma, respectively. This implies that the source terrains now being eroded first cooled through the muscovite closure temperature 350°–400°C (~11–13 km) relatively quickly during the early Miocene, but that the sources did not pass through the 250°–350°C (8–11 km) range until after 15 Ma.

[22] All the muscovite grains and all but two of the biotite grains give ages that postdate the consensus India-Asia collision age at this longitude of ~50 Ma [e.g., *Garzanti et al.*, 1987; *Rowley*, 1996; *Searle et al.*, 1987; *Garzanti and van Haver*, 1988]. This requires that the overwhelming majority of the sediment carried by the Indus River was eroded from source terrains deformed and exhumed as a result of the collision between India and Asia. The Precambrian Indian Shield and its cover, even that deformed in the Lesser Himalaya, can thus be eliminated as major sediment sources.

[23] These detrital mica ages can be compared with those measured from the distal Bengal Fan at ODP Site 717, located in the eastern Indian Ocean south of Sri Lanka [*Copeland et al.*, 1990; *Copeland and Harrison*, 1990]. Figure 6 shows that mica ages in the most recent sediments analyzed from the Bengal Fan (1.9–2.7 Ma) are typically younger than those in the Indus River, showing a principal

mode at 10–15 Ma. This shows that these river systems are draining sources with different exhumation histories. Both the Bengal Fan and the Indus River show some mica ages that are close to, or within error of, the depositional age, indicating that they are, and have been, eroding sources which are being rapidly exhumed from depth >11 km, although these do not do not dominate either erosional flux. The bulk of the Indus River muscovites fall within the range 15–25 Ma. If we assume steady state cooling and assume an initial geothermal gradient around 30°C/km and allowing for the effects of advection [*Stüwe et al.*, 1994; *Moore and England*, 2000], these ages equate to source exhumation rates of 450–900 m/m.y. This is much lower than the peak rates between 3–7 km/m.y. estimated from potential sources in the SKMB [e.g., *Villa et al.*, 1996] or the Nanga Parbat-Haramosh Massif where the majority of bedrock mica ages are <10 Ma [*Treloar et al.*, 2000; *Moore and England*, 2000]. Our age data indicates that these areas, though tectonically very active and extremely elevated, do not generate a large proportion of the total bedload, though they must be the sources for the grains dated at <10 Ma. This is consistent with models that propose the cooling at Nanga Parbat is primarily tectonically driven [*Hubbard et al.*, 1995; *Treloar et al.*, 2000].

[24] The provenance of the Indus River can be constrained by comparison of our detrital mica ages with those measured from basement rocks in the drainage basin. In this study we compile Greater Himalaya ages from *Maluski et al.* [1988], *Searle et al.* [1992], *Metcalfe* [1993], *Walker et al.* [1999], *Guillot et al.* [1999], *Stephenson et al.* [2001], and *Stüwe and Foster* [2001]. Ages from the Pakistan Himalaya, west of Nanga Parbat come from the work of *Fontan et al.* [2000] and *Treloar and Rex* [1990], while the Karakoram are constrained from *Searle et al.* [1989], *Villa et al.* [1996], *Krol et al.* [1996b], and *Brookfield and Reynolds* [1990]. Kohistan-Ladakh Batholith exhumation was dated by *George et al.* [1995], *Villa et al.* [1996], *Dunlap and Wysoczanski* [2002], and *Clift et al.* [2002b]. Age constraints for the Nanga Parbat-Haramosh Massif were derived from *Zeitler* [1985], *Zeitler et al.* [1989], *Winslow et al.* [1996], *George et al.* [1995], and *Treloar et al.* [2000].

[25] The age spectra of these different sources are shown in Figure 7. In terms of the muscovite ages the detrital grains are compatible with erosion from the Greater Himalaya, but seem to preclude a dominant flux from either Nanga Parbat or the Pakistan Himalaya. The lack of basement age data means that the contribution of the Karakoram cannot be judged from this mineral group alone. Muscovite ages from the Pakistan Himalaya seem to be generally older than the bulk of those in the river, indicating that this source is not dominant, although it may be the only source capable of producing the grains dated at 30–35 Ma. The dominance of 0–15 Ma biotite ages indicates that erosion from a combination of the Karakoram, Greater Himalaya and Nanga Parbat is inferred. Although the grains <5 Ma would seem to require significant erosion of Nanga Parbat, some of this material may also be coming from fast exhuming terranes in the Karakoram for which little biotite $^{39}Ar/^{40}Ar$ age data exist. The lack of young muscovite grains seems to preclude Nanga Parbat from being a major sediment generator. Peak biotite ages in the Greater Himalaya and Karakoram provide strong overlap, consistent with their expected controlling role in sediment formation. The Kohistan Arc has several age determinations that match river grain ages, but also scatters to older values that are not seen in TH-1 [*Krol et al.*, 1996a], indicating that this unit is not the prime sediment source.

[26] The $^{39}Ar/^{40}Ar$ age distribution of detrital biotite and muscovite grains from TH-1 can thus be interpreted to reflect dominant erosion in the modern river from the Greater Himalaya and Karakoram, with lesser input from Nanga Parbat and the Pakistan Himalaya. Recycling from older foreland sediments may occur but is not a dominant part of the bedload.

5. Apatite Fission Track Analysis

[27] The apatite fission track results are shown graphically as a radial plot in Figure 8, allowing both the age and the uncertainty of any given grain to be assessed. The FT data are limited by the low number of analyzable grains (only 19), which also prevented track length measurement. Nevertheless, two distinct age populations were found in sample TH-1 and these are shown on the radial plot. The oldest mode at $\sim$14 $\pm$ 4 Ma comprises only three grain ages, while the dominant group at 2.2 $\pm$ 0.6 Ma contains 16 grain ages. The older mode implies a relatively stable source that has experienced moderately low rates of exhumation ($\leq$200 m/m.y.). In contrast, the exhumation rates for the dominant younger mode must have been much faster and closer to 1 km/m.y. (allowing for advection effects). The rate of exhumation inferred by the bulk of the FT data ($\sim$1 km/m.y.) is slightly faster than for the argon data (450–900 m/m.y.). Assuming the apatite and mica grains are derived from the same terrain this difference suggests a recent (prior to 2 Ma) acceleration in exhumation, probably starting since the Pliocene. The significant number of biotite ages <10 Ma also supports the idea of faster exhumation starting in the recent geologic past, especially since the late Miocene.

[28] Such a change in exhumation rates might also reflect different sensitivity of each method to different processes. Mica (especially muscovite) ages are more closely linked to deeper, crustal-scale faulting and tectonic denudation, while the lower temperature apatite FT system is more sensitive to surficial processes such as enhanced fluvial and glacial erosion. A post-Pliocene acceleration in erosion rates is consistent with the model of *Zhang et al.* [2001] that linked faster continental erosion and a more intense glacial climate after $\sim$4 Ma. It is also noteworthy that *Clift et al.* [2003] recorded a moderate increase in Pleistocene sedimentation rates on the Indus Fan over the same time period.

[29] As with the other mineral thermochronometers a difference is observed between the Indus River and the Bengal Fan. The latter showed an average age of 4.8 Ma for the Pleistocene sediments sampled at ODP Site 717 [*Corrigan and Crowley*, 1990]. The age spectra of single grain ages are shown in Figure 9, where the Indus and Bengal

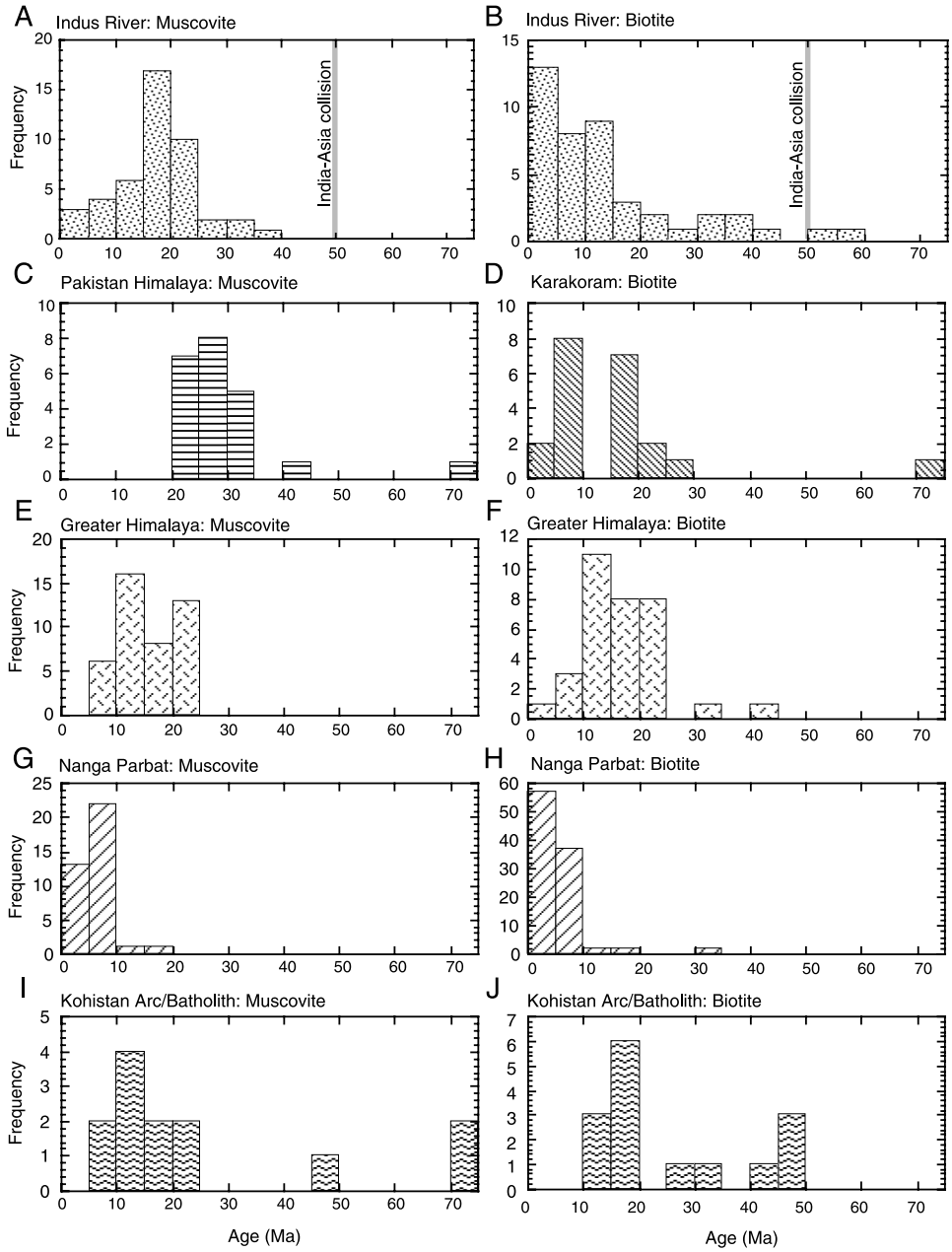

Figure 7. Range of $^{39}Ar/^{40}Ar$ ages measured from Indus River (a) muscovites and (b) biotites, compared to those known from major possible source terrains in the modern drainage, including (c) Pakistan Himalaya, (d) Karakoram, (e) Greater Himalayan muscovites and (f) biotites, Nanga Parbat (g) muscovites and (h) biotites, and Kohistan (i) muscovites and (j) biotites. Sources of basement data are provided in text.

systems are compared, together with basement data from the Greater Himalaya [*Kumar et al.*, 1995; *Sorkhabi et al.*, 1996; *Searle et al.*, 1997; *Jain et al.*, 2000; *Stüwe and Foster*, 2001], Nanga Parbat [*Zeitler*, 1985; *Warner*, 1993; *Foster et al.*, 1994; *Treloar et al.*, 2000], Pakistan Himalaya [*Zeitler*, 1985] and the Karakoram [*Carpena and Rutkiewicz*, 1989; *Poupeau et al.*, 1991; *Foster et al.*, 1994]. Ages from the Kohistan Arc are from *Zeitler* [1985] and *Zeilinger et al.* [2001].

[30] The limited fission track data show at least two sources exhuming at different rates are contributing to the Indus River and that these differ from those feeding the geologically recent Bengal Fan. The older minority set of fission track ages (~14 Ma) is comparable to data from the Kohistan Arc or Pakistan Himalaya, though other possible sources include the Greater Himalaya [*Searle et al.*, 1997]. Young apatite FT ages have been recorded in the region of K2 in the Karakoram (2.1–4.3 Ma [*Foster et al.*, 1994]) and in

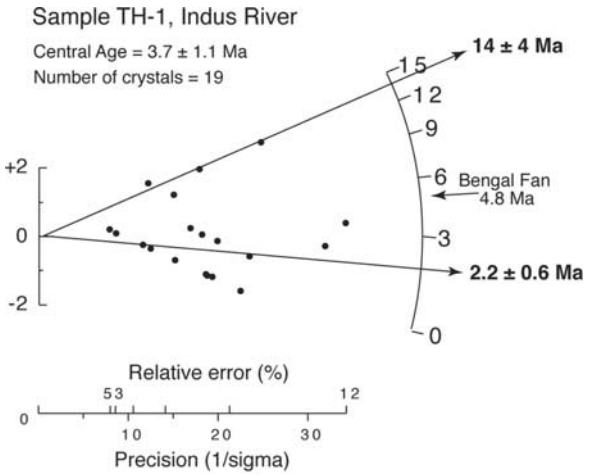

Figure 8. Radial plot of apatite fission track data showing the spread of ages and the uncertainties associated with each grain. Two peaks in age are resolved, suggesting mixing of sediment from at least two sources. Note 4.8 Ma peak in Pleistocene Bengal Fan sediment that has no equivalent in the Indus River.

the SKMB (0.8–3.8 Ma [*Poupeau et al.*, 1991]). It is clear that grains eroded from these regions must be delivered to the modern Indus River, and that the SKMB may be a source of young apatites to the Indus. In contrast the Karakoram Batholith has been experiencing much slower exhumation (rates of <1km/m.y. [*Krol et al.*, 1996b], resulting in slightly older fission track ages of ~3–5 Ma inconsistent with the younger grains seen in TH-1. Another possible source area is the Nanga Parbat-Haramosh Massif. However, here exhumation rates are extremely high (>2 km/m.y.) and most of the recorded FT ages are too young at <1 Ma. The other mineral groups discussed above also argue against Nanga Parbat being a dominant source. The Greater Himalaya are capable of providing the large number of grains with ages <3 Ma. In particular, analyses of rocks in the upper Sutlej Valley [*Jain et al.*, 2000; *Vannay et al.*, 2003] demonstrate that suitable sources exist in the Indus drainage to provide such grains to the lower reaches of the river. Given the constraints from the zircon and mica dating it seems likely that the SKMB and especially the Greater Himalaya are the major sources of young apatite grains to sample TH-1.

[31] In conclusion, the mostly young (2.2 Ma) apatite fission track ages from the lower Indus River are compatible with a dominant provenance from the Greater Himalaya and to a lesser extent the SKMB. Mica Ar-Ar ages and geochemistry argue against a dominant role for the Nanga Parbat-Haramosh Massif. The older minority set of fission track ages (~14 Ma) are more similar to those known from the Kohistan Arc or Pakistan Himalaya, though suitable sources are also known in the Greater Himalaya [*Searle et al.*, 1997].

6. Contribution of Recycled Sediments

[32] A fundamental uncertainty is the contribution of recycled sediment derived from older foreland sequences to the modern bedload. Previous studies that have determined Ar-Ar ages from detrital mica from the Neogene Dharamsala Formation and Siwalik Group of the Indo-Pakistani foreland basin showed a wide range of ages, extending from the Proterozoic to Neogene [e.g., *White et al.*, 2002; *Najman et al.*, 1997]. The age distribution of mica ages in the foreland sediments is closely similar to those in the modern Indus (Figure 6) and might imply that some of the Indus sediments derive from foreland sources. However, only two of the Indus River muscovite ages are older than 70 Ma, contrasting with the foreland mica ages, which have a significant component of grains older than 200 Ma (e.g., Figure 6 [*White et al.*, 2002]). The absence of old mica ages from the sample TH-1 strongly suggests that little if any material is being recycled from foreland sources.

[33] The Neogene Siwalik Group, deposited within the modern drainage of the Indus, shows a range of muscovite ages that seem to predate their depositional age of 12.5 Ma by ~10 m.y. (Figure 6d [*White et al.*, 2002]), a pattern which is closer to the modern Bengal Fan than the Indus Fan. However, older Siwalik Group sediments deposited at 17 Ma and 20.5 Ma (Figures 7e and 7f) show cooling ages that are even closer to the age of deposition [*White et al.*, 2002], implying faster source exhumation at that time compared to the modern state. Micas from the early Miocene Dharamsala Formation show a maximum number of cooling ages that are only slightly older than the age of sedimentation [*Najman et al.*, 1997], implying the fastest exhumation rates. The ages of modern Indus River micas are thus consistent with a gradual slowing of source exhumation rates in the Indus drainage basin since the early Miocene.

7. Implications for Continental Genesis

[34] By sampling wide areas of crust in south Asia the Indus River allows broad patterns of continental evolution to be reconstructed, drawing on all three of the mineral groups considered here. U-Pb ages for zircon show that only small amounts of the total crust now being eroded was melted during India-Asia collision-related magmatism, deformation and metamorphism, totally only seven of the 132 grains analyzed (~5%), all likely from the Karakoram and/or Kohistan Batholith. Another 21 grains (16%) were of Mesozoic age and reflect active margin magmatism along the southern margin of Asia prior to collision. The substantial majority of the crust (69%) is of Precambrian origin. Conversely, because practically all the detrital mica ages are postcollisional and most of the apatite fission track ages are ~2 Ma we can see that the sediment source regions, i.e., the mountains, not the Indian Shield, have been strongly thermally reset by collision.

8. Implications for the Deep-Sea Marine Record

[35] The new detrital age data for the modern Indus River presented here suggests that the bedload of the river is dominated by material from areas undergoing strong ero-

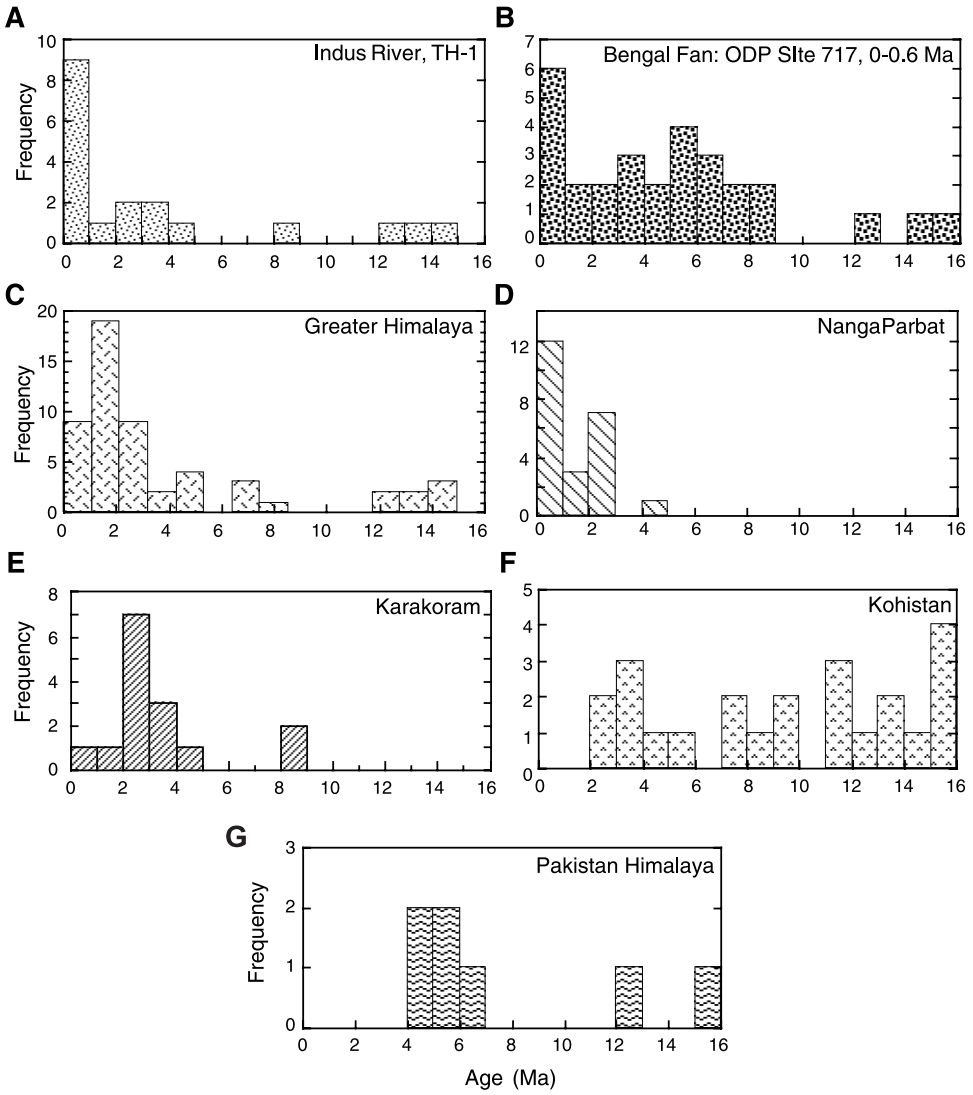

Figure 9. Frequency histograms for apatite fission track ages of single grains, divided into 1 m.y. bins from (a) the Indus River at TH-1 and (b) the Bengal Fan (data from *Corrigan and Crowley* [1990]). Both systems show a recent peak in values, but the 5–6 Ma maximum in the Bengal Fan is not seen in the new Indus data. Apatite fission track ages are also shown for the (c) Greater Himalaya, (d) Nanga Parbat, (e) the Karakoram, (f) Kohistan and (g) Pakistan Himalaya.

sion, which correlates with regions that have the highest topography and most relief [*Finlayson et al.*, 2002] within the modern catchment, i.e., from the Karakoram and Greater Himalaya. Erosion of material from the Lesser Himalaya and recycling of sediment from older foreland basin sequences accounts for only a small fraction of the total bedload reaching the Arabian Sea. Similarly, if sediment is being sequestered and temporarily stored on the Indus floodplain before delivery to the Arabian Sea this is either volumetrically insignificant or must be occurring on shorter timescales than the youngest ages (i.e., <2 m.y.).

[36] The thermochronometric provenance constraints have to be considered in the light of Nd and Pb isotopic provenance controls from the Indus River, which favored a dominance by the Karakoram over the Greater Himalaya in providing material to the deep sea Indus Fan [*Clift et al.*, 2002a], a pattern that is not apparent here. However, in that study sample TH-1 was seen to differ from sediments taken from higher parts of the modern drainage, or from older Indus Fan sediments from the Arabian Sea. Further analyses are required from the lower reaches in order to determine if TH-1 is truly representative of the bedload now being delivered into the Arabian Sea. The bulk sediment Nd isotopic character of TH-1 is much more radiogenic than is typical for the historical Indus system, $\varepsilon_{Nd} = -15.5$, compared to -10.8 just above the Tarbela Dam, and -12.5 to -14.0 at ODP Site 720 on the Indus Fan (Figure 1), implying a disproportionately large influence from the Greater Himalaya relative to the Karakoram in TH-1 [*Clift et al.*, 2002a]. If sample TH-1 is representative of the bedload then the lower reaches today

have more material delivered by the Himalaya-draining tributaries (Sutlej, Jellum, Chenab, and Ravi) than can have been the case for most geological time. The reasons for this strong Greater Himalayan flux may be linked to the damming of the main Indus River at Tarbela and other locations. Our thermochronology study is consistent with the isotopic provenance constraints in showing a strong Greater Himalayan signal in TH-1, although a Karakoram signature is still apparent and resolvably different within the mixed sediment of the lower river.

[37] The implications of this study, that the Indus bedload is strongly biased toward areas of highest erosion and topography has important implications for our ability to use the marine sedimentary record to reconstruct the growth of topography onshore. Although the influence of the Lesser Himalaya and recycled foreland sediments (Siwalik, Dharamsala, and Kasauli Formations) to the three different mineral budgets is difficult to robustly assess, it is clear, based on these results, that they can only form a relatively minor components of the total flux. This means that the deep sea fan sediments should retain a clear signal of regional topographic growth in the western Himalaya and Karakoram.

9. Conclusions

[38] This study has demonstrated the benefits of combining several thermochronometers to study the provenance of sediments. The combination of U-Pb dating of zircon grains, $^{39}Ar/^{40}Ar$ dating of micas and fission track analysis of apatites taken from river sand from the lower Indus River provide important new insights on the provenance of this drainage. U-Pb dates show a mixed provenance of material, eroded from the Greater Himalaya, together with inputs from the Karakoram and Lesser Himalaya, including small volumes of recycled foreland sediment. Mica ages show a strong distinction between the Indus and Bengal Fan systems, reflecting the different exhumation histories in their drainage basins. Mica ages are typically younger in micas from the Bengal Fan than from the Indus River, reflecting the different tectonic histories of the source terrains. The 15–25 Ma peak in muscovite $^{39}Ar/^{40}Ar$ ages in Indus River sediment indicates that the sources of detritus to the bedload have not been exhuming at very fast rates since the early Miocene, when it was at its peak. In contrast, younger biotite $^{39}Ar/^{40}Ar$ and apatite fission track ages suggest that erosion rates have increased since the late Miocene-Pliocene. The long term exhumation rates implied by the fission track and $^{39}Ar/^{40}Ar$ dating are somewhat slower than the highest rates measured in limited areas of the Nanga Parbat-Haramosh Massif and SKMB, indicating that such sources do not dominate the sedimentary record. Conversely the lack of very old mica and fission track ages implies that the Indian Shield, Lesser Himalaya, and foreland sediments are not major suppliers of sediment.

[39] The sediment reaching the Arabian Sea as bedload to the Indus River thus appears to be dominated by sources derived from the highest ranges in the modern catchment. This suggests that the geological record of erosion stored in the sediments of the Indus Fan contains a recoverable signal of the growth of the western Himalaya. This resource provides the best opportunity for reconstructing Himalayan topographic relief evolution essential for testing climate models that link monsoon strength to topographic uplift in south Asia.

[40] **Acknowledgments.** Scottish Universities Environmental Research Centre (SUERC) is supported by the Scottish Universities and the British National Environmental Research Council (NERC). P. C. wishes to thank the Joint Oceanographic Institutions (JOI) for partial support of this work.

References

Anczkiewicz, R., F. Oberli, J. P. Burg, I. M. Villa, D. Günther, and M. Meier (2001), Timing of normal faulting along the Indus Suture in Pakistan Himalaya and a case of major $^{231}Pa/^{235}U$ initial disequilibrium in zircon, *Earth Planet. Sci. Lett.*, *191*, 101–114.

Ballard, J. R., J. M. Palin, I. S. Williams, I. H. Campbell, and A. Faunes (2001), Two ages of porphyry intrusion revealed for the super-giant Chuquicamata copper deposits of northern Chile by ELA-ICP-MS and SHRIMP, *Geology*, *29*, 383–386.

Black, L. P., S. L. Kamo, I. S. Wiliiams, C. Foudoulis, J. C. Claoue-Long, R. J. Korsch, and D. W. Davis (2000), The quest for a high quality zircon standard for microbeam Pb-U-Th geochronology, in *Searching for a Sustainable Future: 15th Australian Geological Convention*, *Abstr. Geol. Soc. Aust.*, vol. 59, p. 43, Geol. Soc. of Aust., Sydney.

Brookfield, M. E., and P. H. Reynolds (1990), Miocene $^{40}Ar/^{39}Ar$ ages from the Karakorum Batholith and Shyok Melange, northern Pakistan, indicate late Tertiary uplift and southward displacement, *Tectonophysics*, *172*, 155–167.

Carpena, J., and W. Rutkiewicz (1989), Ages traces de fission des apatites et des zircons du sommet du K2 (8611 m), Pakistan, *Eclogae Geol. Helv.*, *82*(3), 735–742.

Carter, A. (1999), Present Status and future avenues of source region discrimination and characterisation using fission-track analysis, *Sediment Geol.*, *124*, 31–45.

Carter, A., and C. S. Bristow (2000), Detrital zircon geochronology: Enhancing the quality of sedimentary source information through improved methodology and combined U-Pb and fission track techniques, *Basin Res.*, *12*, 47–57.

Cherniak, D. J., and E. B. Watson (2001), Pb diffusion in zircon, *Chem. Geol.*, *172*, 5–24.

Clift, P. D., J. I. Lee, P. Hildebrand, N. Shimizu, G. D. Layne, J. Blusztajn, J. D. Blum, E. Garzanti, and A. A. Khan (2002a), Nd and Pb isotope variability in the Indus River system: Implications for sediment provenance and crustal heterogeneity in the western Himalaya, *Earth Planet. Sci. Lett.*, *200*, 91–106.

Clift, P. D., A. Carter, M. Krol, and E. Kirby (2002b), Constraints on India-Eurasia collision in the Arabian Sea region taken from the Indus Group, Ladakh Himalaya, India, in *The Tectonic and Climatic Evolution of the Arabian Sea Region*, edited by P. D. Clift et al., *Geol. Soc. Spec. Publ.*, *195*, 97–116.

Clift, P. D., C. Gaedicke, R. Edwards, J. I. Lee, P. Hildebrand, S. Amjad, R. S. White, and H. U. Schülter (2003), The stratigraphic evolution of the Indus Fan and the history of sedimentation in the Arabian Sea, *Mar. Geophys. Res.*, *93*(2), 101–110.

Compston, W., I. S. Williams, and C. E. Meyer (1984), Unsupported radiogenic Pb in zircon: A case for anomalously high Pb-Pb, U-Pb and Th-Pb age, *Contrib. Mineral. Petrol.*, *88*, 322–327.

Copeland, P., and T. M. Harrison (1990), Episodic rapid uplift in the Himalaya revealed by $^{40}Ar/^{39}Ar$ analysis of detrital K-feldspar and muscovite, Bengal fan, *Geology*, *18*, 354–357.

Copeland, P., T. M. Harrison, and M. T. Heizler (1990), $^{40}Ar/^{39}Ar$ single-crystal dating of detrital muscovite and K-feldspar from Leg 116, southern Bengal fan: Implications for the uplift and erosion of the Himalayas, *Proc. Ocean Drill. Program Sci. Results*, *116*, 93–114.

Corrigan, J. D., and K. D. Crowley (1990), Fission track analysis of detrital apatites from Sites 717 and 718, Leg 116, central Indian Ocean, *Proc. Ocean Drill. Program Sci. Results*, *116*, 75–92.

Cumming, G. L., and J. R. Richards (1975), Ore lead isotope ratios in a continuously changing Earth, *Earth Planet. Sci. Lett.*, *28*, 155–171.

DeCelles, P. G., G. E. Gehrels, J. Quade, B. LaReau, and M. Spurlin (2000), Tectonic implications of U-Pb zircon ages of the Himalayan orogenic belt in Nepal, *Science*, *288*(5465), 497–499.

Dunlap, W. J., and R. Wysoczanski (2002), Thermal evidence for Early Cretaceous metamorphism in the Shyok suture zone and age of the Khardung volcanic rocks, Ladakh, India, *J. Asian Earth Sci.*, *20*(5), 481–490.

Finlayson, D. P., D. R. Montgomery, and B. Hallet (2002), Spatial coincidence of rapid inferred erosion with young metamorphic massifs in the Himalayas, *Geology*, *30*, 219–222.

Fontan, D., M. Schouppe, C. J. Hunziker, G. Martinotti, and J. Verkaeren (2000), Metamorphic evolution, ^{40}Ar-^{39}Ar chronology and tectonic model for the Neelum Valley, Azad Kashmir, NE Pakistan, in *Tectonics of the Nanga Parbat Syntaxis and the Western Himalaya*, edited by M. A. Khan et al., *Geol. Soc. Spec. Publ.*, *170*, 431–453.

Foster, D. A., A. J. W. Gleadow, and G. Mortimer (1994), Rapid Pliocene exhumation in the Karakoram (Pakistan), revealed by fission-track thermochronology of the K2 gneiss, *Geology*, *22*, 19–22.

Fraser, J. E., M. P. Searle, R. R. Parrish, and S. R. Noble (2001), Chronology of deformation, metamorphism, and magmatism in the southern Karakoram Mountains, *Geol. Soc. Am. Bull.*, *113*, 1443–1455.

Galy, A., and C. France-Lanord (2001), Higher erosion rates in the Himalaya: Geochemical constraints on riverine fluxes, *Geology*, *29*, 23–26.

Garzanti, E., and T. van Haver (1988), The Indus clastics: Forearc basin sedimentation in the Ladakh Himalaya (India), *Sediment. Geol.*, *59*, 237–249.

Garzanti, E., A. Baud, and G. Mascle (1987), Sedimentary record of the northward flight of India and its collision with Eurasia (Ladakh Himalaya, India), *Geodin. Acta*, *1*(4/5), 297–312.

George, M., S. Reddy, and N. Harris (1995), Isotopic constraints on the cooling history of the Nanga Parbat-Haramosh Massif and Kohistan Arc, western Himalaya, *Tectonics*, *14*, 237–252.

Green, P. F., I. R. Duddy, G. M. Laslett, K. A. Hegarty, A. J. W. Gleadow, and J. F. Lovering (1989), Thermal annealing of fission tracks in apatite: 4 quantitative modeling techniques and extension to geological timescales, *Chem. Geol.*, *79*, 155–182.

Guillot, S., M. Cosca, P. Allemand, P. Le Fort (1999), Contrasting metamorphic and geochronologic evolution along the Himalayan belt, in *Himalaya and Tibet: Mountain Roots to Mountain Tops*, edited by A. Macfarlane, R. B. Sorkharbi, and J. Quade, *Spec. Pap. Geol. Soc. Am.*, *328*, 117–128.

Harrison, T. M., P. Copeland, W. S. F. Kidd, and A. Yin (1992), Raising Tibet, *Science*, *255*, 1663–1670.

Hirata, T., and R. W. Nesbitt (1995), U-Pb isotope geochronology of zircon: Evaluation of the laser probe-inductively coupled plasma mass spectrometer technique, *Geochim. Cosmochim. Acta*, *59*, 2491–2500.

Hodges, K. V. (2003), Geochronology and thermochronology in orogenic systems, in *Treatise on Geochemistry: The Crust*, edited by R. L. Rudnick, pp. 263–292, Elsevier Sci., New York.

Hodges, K. V., and S. A. Bowring (1995), ^{40}Ar/^{39}Ar thermochronology of isotopically zoned micas: Insight from the southwestern USA Proterozoic orogen, *Geochim. Cosmochim. Acta*, *59*, 3205–3220.

Hodges, K. V., R. R. Parrish, and M. P. Searle (1996), Tectonic evolution of the central Annapurna Range, Nepalese Himalayas, *Tectonics*, *15*, 1264–1291.

Honegger, K., V. Dietrich, W. Frank, A. Gansser, M. Thoeni, and V. Trommsdorff (1982), Magmatism and metamorphism in the Ladakh Himalayas (the Indus-Tsangpo suture zone), *Earth Planet. Sci. Lett.*, *60, 253–292.*

Horn, I., R. L. Rudnick, and W. F. McDonough (2000), Precise elemental and isotope ratio determination by simultaneous solution nebulization and laser ablation ICP-MS: Application to U-Pb geochronology, *Chem. Geol.*, *164*, 281–301.

Hubbard, M. S., D. A. Spencer, and D. P. West (1995), Tectonic exhumation of the Nanga Parbat Massif, northern Pakistan, *Earth Planet. Sci. Lett.*, *133*, 213–225.

Jain, A. K., D. Kumar, S. Singh, A. Kuma, and N. Lal (2000), Timing, quantification and tectonic modelling of Pliocene-Quaternary movements in the NW Himalaya: Evidence from fission track dating, *Earth Planet. Sci. Lett.*, *179*, 437–451.

Koppers, A. A. P. (2002), ArArCalc-software for ^{40}Ar/^{39}Ar age calculation, *Comput. Geosci.*, *28*, 605–619.

Krol, M. A., P. K. Zeitler, and P. Copeland (1996a), Episodic unroofing of the Kohistan Batholith, Pakistan: Implications from K-feldspar thermochronology, *J. Geophys. Res.*, *101*, 28,149–28,164.

Krol, M. A., P. K. Zeitler, G. Poupeau, and A. Pecher (1996b), Temporal variations in the cooling and denudation history of the Hunza plutonic complex, Karakoram Batholith, revealed by ^{40}Ar/^{39}Ar thermochronology, *Tectonics*, *15*, 403–415.

Kumar, A., N. Lal, A. K. Jain, and R. B. Sorkhabi (1995), Late Cenozoic-Quaternary thermo-tectonic history of Higher Himalayan Crystalline (HHC) in Kishtwar-Padar-Zanskar region, NW Himalaya: Evidence from fission track ages, *J. Geol. Soc., India*, *45*(4), 375–391.

Lee, J. I., P. D. Clift, G. Layne, J. Blum, and A. A. Khan (2003), Sediment flux in the modern Indus River traced by the trace element composition of detrital amphibole grains, *Sediment. Geol.*, *160*, 243–257.

Le Fort, P., F. Debon, and J. Sonet (1983), Petrography, geochemistry and geochronology of some samples from the Karakoram Batholith (N. Pakistan), in *Granites of the Himalayas, Karakoram and Hindu Kush*, edited by F. A. Shams, pp. 377–387, Punjab Univ., Lahore, Pakistan.

Maluski, H., P. Matte, M. Brunel, and X. Xiao (1988), Argon 39 - Argon 40 dating of metamorphic and plutonic events in the north and High Himalaya belts (southern Tibet-China), *Tectonics*, *7*, 299–326.

Metcalfe, R. P. (1993), Pressure, temperature and time constraints on metamorphism across the Main Central Thrust zone and High Himalayan slab in the Garhwal Himalaya, in *Himalayan Tectonics*, edited by P. J. Treloar and M. P. Searle, *Geol. Soc. Spec. Publ.*, *74*, 485–509.

Molnar, P., P. England, and J. Martinod (1993), Mantle dynamics, the uplift of the Tibetan Plateau, and the Indian monsoon, *Rev. Geophys.*, *31*, 357–396.

Moore, M. A., and P. C. England (2000), On the inference of denudation rates from cooling ages of minerals, *Earth Planet. Sci. Lett.*, *185*, 264–284.

Najman, Y. M. R., M. S. Pringle, M. R. W. Johnson, A. H. F. Robertson, and J. R. Wijbrans (1997), Laser ^{40}Ar/^{39}Ar dating of single detrital muscovite grains from early foreland-basin sedimentary deposits in India: Implications for early Himalayan evolution, *Geology*, *25*, 535–538.

Najman, Y. M. R., M. Pringle, L. Godin, and G. A. Oliver (2002), A reinterpretation of the Balakot Formation: Implications for the tectonics of the NW Himalaya, Pakistan, *Tectonics*, *21*(5), 1045, doi:10.1029/2001TC001337.

Noble, S. R., and M. P. Searle (1995), Age of crustal melting and leucogranite formation from U-Pb zircon and monazite dating in the western Himalaya, Zanskar, India, *Geology*, *23*, 1135–1138.

Parrish, R. R., and K. V. Hodges (1996), Isotopic constraints on the age and provenance of the Lesser and Greater Himalayan sequences, Nepalese Himalaya, *Geol. Soc. Am. Bull.*, *108*, 904–911.

Parrish, R. R., and R. Tirrul (1989), U-Pb age of the Baltoro Granite, northwest Himalaya, and implications for monazite U-Pb systematics, *Geology*, *17*, 1076–1079.

Pearce, N. J. G., W. T. Perkins, J. A. Westgate, M. P. Gorton, S. E. Jackson, C. R. Neal, and S. P. Chenery (1997), A compilation of new and published major and trace element data for NIST SRM 610 and NIST SRM 612 glass reference materials, *Geostand. Newsl.*, *21*, 115–144.

Poupeau, G., A. Pecher, M. Benharbit, and O. F. Noyan (1991), Ages traces de fission sur apatites et taux de denudation plio-quaternaires au Karakorum central: Apatite fission-track dating of the Plio-Quaternary denudation rate in central Karakoram, *C. R. Acad. Sci., Ser. 2*, *313*, 917–922.

Renne, P. R., C. C. Swisher, A. L. Deino, D. B. Karner, T. Owens, and D. J. DePaolo (1998), Intercalibration of standards, absolute ages and uncertainties in ^{40}Ar/^{39}Ar dating, *Chem. Geol.*, *145*, 117–152.

Rowley, D. B. (1996), Age of initiation of collision between India and Asia: A review of stratigraphic data, *Earth Planet. Sci. Lett.*, *145*, 1–13.

Schärer, U., J. Hamet, and C. J. Allegre (1984), The Transhimalaya (Gangdese) plutonism in the Ladakh region: A U-Pb and Rb-Sr study, *Earth Planet. Sci. Lett.*, *67*, 327–339.

Schärer, U., P. Copeland, T. M. Harrison, and M. P. Searle (1990), Age, cooling history, and origin of post-collisional leucogranites in the Karakoram Batholith; a multi-system isotope study, *J. Geol.*, *98*(2), 233–251.

Searle, M. P. (1996), Cooling history, erosion, exhumation and kinematics of the Himalaya-Karakorum-Tibet orogenic belt, in *The Tectonic Evolution of Asia*, edited by A. Yin and T. M. Harrison, pp. 110–137, Cambridge Univ. Press, New York.

Searle, M. P., et al. (1987), The closing of Tethys and the tectonics of the Himalaya, *Geol. Soc. Am. Bull.*, *98*, 678–701.

Searle, M. P., A. J. Rex, R. Tirrul, D. C. Rex, A. C. Barnicoat, and B. F. Windley (1989), Metamorphic, magmatic, and tectonic evolution of the central Karakoram in the Biafo-Baltoro-Hushe regions of northern Pakistan, in *Tectonics of the Western Himalayas*, edited by L. L. Malinconico and R. J. Lillie, *Spec. Pap. Geol. Soc. Am.*, *232*, 47–73.

Searle, M. P., R. R. Parrish, R. Tirrul, and D. C. Rex (1990), Age of crystallization of the K2 gneiss in the Baltoro Karakoram, *J. Geol. Soc. London*, *147*, 603–606.

Searle, M. P., D. J. Waters, D. C. Rex, and R. N. Wilson (1992), Pressure, temperature and time constraints on Himalayan metamorphism from eastern Kashmir and western Zanskar, *J. Geol. Soc. London*, *149*, 753–773.

Searle, M. P., R. R. Parrish, K. V. Hodges, A. Hurford, M. W. Ayres, and M. J. Whitehouse (1997), Shisha Pangma leucogranite, south Tibetan Himalaya: Field relations, geochemistry, age, origin, and emplacement, *J. Geol.*, *105*(3), 295–317.

Sorkhabi, R., A. K. Jain, S. Nishimura, T. Itaya, N. Lal, R. M. Manickavasagam, and T. Tagami (1994), New age constraints on the cooling and unroofing of the Trans-Himalayan Ladakh Batholith (Kargil area), NW India, *Proc. Indian Acad. Sci. Earth Planet. Sci.*, *103*, 83–97.

Sorkhabi, R. B., E. Stump, K. A. Foland, and A. K. Jain (1996), Fission-track and ^{40}Ar/^{39}Ar evidence for episodic denudation of the Gangotri granites in the Garhwal Higher Himalaya, India, *Tectonophysics*, *260*, 187–199.

Stephenson, B. J., M. P. Searle, D. J. Waters, and D. C. Rex (2001), Structure of the Main Central Thrust zone and extrusion of the High Himalayan deep crustal wedge, Kishtwar-Zanskar Himalaya, *J. Geol. Soc. London*, *158*, 637–652.

Stüwe, K., and D. Foster (2001), ^{40}Ar/^{39}Ar, pressure, temperature and fission track constraints on the age and nature of metamorphism around the main central thrust in the eastern Bhutan Himalaya, *J. Asian Earth Sci.*, *19*(1–2), 85–95.

Stüwe, K., L. White, and R. Brown (1994), The influence of eroding topography on steady-state isotherms: Application to fission track analysis, *Earth Planet. Sci. Lett.*, *124*, 63–74.

Treloar, P. J., and D. C. Rex (1990), Post-metamorphic cooling history of the Indian plate crystalline thrust stack, Pakistan Himalaya, *J. Geol. Soc. London*, *147*, 735–738.

Treloar, P. J., D. C. Rex, P. G. Guise, J. Wheeler, A. J. Hurford, and A. Carter (2000), Geochronological constraints on the evolution of the Nanga Parbat syntaxis, Pakistan Himalaya, in *Tectonics of the*

Nanga Parbat Syntaxis and the Western Himalaya, edited by M. A. Khan et al., *Geol. Soc. Spec. Publ.*, *170*, 137–162.

Vannay, J. C., B. Grassman, M. Rahn, W. Frank, and A. Carter (2003), Active tectonics coupled to fluvial erosion in the NW Himalaya, *Geophys. Res. Abstr.*, *5*, Abstract EAE03-A-03988.

Villa, I. M., Y. Lemennicier, and P. Le Fort (1996), Late Miocene to early Pliocene tectonometamorphism and cooling in south-central Karakorum and Indus-Tsangpo suture, Chogo Lungma area (NE Pakistan), *Tectonophysics*, *260*, 201–214.

Walker, J. D., M. W. Martin, S. A. Bowring, M. P. Searle, D. J. Waters, and K. V. Hodges (1999), Metamorphism, melting, and extension: Age constraints from the High Himalayan slab of Southeast Zanskar and Northwest Lahaul, *J. Geol.*, *107*(4), 473–495.

Warner, L. F. (1993), Variable denudation of the Nanga Parbat-Haramosh Massif: A fission track study of the Tato Valley, Pakistan, senior thesis, 34 pp., Lehigh Univ., Bethlehem, PA.

Weinberg, R. F., and W. J. Dunlap (2000), Growth and deformation of the Ladakh Batholith, northwest Himalayas: Implications for timing of continental collision and origin of calc-alkaline batholiths, *J. Geol.*, *108*(3), 303–320.

White, N. M., M. Pringle, E. Garzanti, M. Bickle, Y. Najman, H. Chapman, and P. Frien (2002), Constraints on the exhumation and erosion of the High Himalayan slab, NW India, from foreland basin deposits, *Earth Planet. Sci. Lett*, *195*, 29–44.

Winslow, D. M., P. K. Zeitler, C. P. Chamberlain, and I. S. Williams (1996), Geochronologic constraints on syntaxial development in the Nanga Parbat region, Pakistan, *Tectonics*, *15*, 1292–1308.

Zeilinger, G., J. P. Burg, U. Schaltegger, and D. Seward (2001), New U/Pb and fission track ages and their implication for the tectonic history of the lower Kohistan Arc Complex, northern Pakistan, *J. Asian Earth Sci.*, *19*, 79–81.

Zeitler, P. K. (1985), Cooling history of the NW Himalaya, Pakistan, *Tectonics*, *4*, 127–151.

Zeitler, P. K., and C. P. Chamberlain (1991), Petrogenetic and tectonic significance of young leucogranites from the northwestern Himalaya, Pakistan, *Tectonics*, *10*, 729–741.

Zeitler, P. K., J. F. Sutter, I. S. Williams, R. E. Zartman, and R. A. K. Tahirkheli (1989), Geochronology and temperature history of the Nanga Parbat-Haramosh Massif, Pakistan, in *Tectonics of the Western Himalayas*, edited by L. L. Malinconico and R. J. Lillie, *Spec. Pap. Geol. Soc. Am.*, *232*, 1–22.

Zeitler, P. K., C. P. Chamberlain, and H. A. Smith (1993), Synchronous anatexis, metamorphism and rapid denudation at Nanga Parbat (Pakistan Himalaya), *Geology*, *21*, 347–350.

Zeitler, P. K., et al. (2001), Erosion, Himalayan geodynamics and the geomorphology of metamorphism, *GSA Today*, *11*, 4–9.

Zhang, P., P. Molnar, and W. R. Downs (2001), Increased sedimentation rates and grain sizes 2–4 Myr ago due to the influence of climate change on erosion rates, *Nature*, *410*, 891–897.

C. M. Allen and I. H. Campbell, Institute of Advanced Studies, Research School of Earth Sciences, Australian National University, Canberra, ACT 0200, Australia. (charlotte.allen@anu.edu.au; ian.campbell@anu.edu.au)

A. Carter, School of Earth Sciences, University and Birkbeck College London, Gower Street, London WC1E 6BT, UK. (a.carter@ucl.ac.uk)

P. D. Clift, Department of Geology and Petroleum Geology, Kings College, Meston Building, University of Aberdeen, Aberdeen AB24 3UE, UK. (p.clift@abdn.ac.uk)

K. V. Hodges and M. S. Pringle, Department of Earth, Atmospheric and Planetary Sciences, Massachusetts Institute of Technology, Cambridge, MA 02139-4307, USA. (kvhodges@mit.edu; mpringle@mit.edu)

A. A. Khan, Department of Geology, University of Karachi, Karachi-75270, Pakistan. (athargeo@super.net.pk)

X. Zhang, Department of Geology and Geophysics, University of Wisconsin-Madison, 1215 Dayton Street, Madison, WI 53706, USA.